TOPICAL REVIEW — Iron-based high temperature superconductors

Interplay of superconductivity and d–f correlation in $CeFeAs_{1-x}P_xO_{1-y}F_y$*

Luo Yong-Kang(罗永康)[a], Li Yu-Ke(李玉科)[a)b)], Wang Cao(王 操)[a)c)], Lin Xiao(林 效)[a)], Dai Jian-Hui(戴建辉)[a)b)], Cao Guang-Han(曹光旱)[a)], and Xu Zhu-An(许祝安)[a)†]

[a)] *Department of Physics and State Key Laboratory of Silicon Materials, Zhejiang University, Hangzhou* 310027, *China*
[b)] *Department of Physics, Hangzhou Normal University, Hangzhou* 310036, *China*
[c)] *Department of Physics, School of Science, Shandong University of Technology, Zibo* 255049, *China*

(Received 8 June 2013; revised manuscript received 15 July 2013)

The recent discovery of high-temperature superconductivity in iron-based pnictides (chalcogenides) not only triggers tremendous enthusiasm in searching for new superconducting materials, but also opens a new avenue to the study of the Kondo physics. CeFeAsO is a parent compound of the 1111-type iron-based superconductors. It shows 3d-antiferromagnetic (AFM) ordering below $\sim$ 139 K and 4f-AFM ordering below $\sim$ 4 K. On the other hand, the phosphide CeFePO is a ferromagnetically correlated heavy-fermion (HF) metal with Kondo scale $T_K \sim 10$ K. These properties set up a new platform for research of the interplay among magnetism, Kondo effect, and superconductivity (SC). In this review, we present the recent progress in the study of chemical pressure effect in $CeFeAsO_{1-y}F_y$ ($y = 0$ and 0.05). This P/As-doping in CeFeAsO serves as an effective controlling parameter which leads to two magnetic critical points, $x_{c1} \simeq 0.4$ and $x_{c2} \simeq 0.92$, associated with suppression of 3d and 4f magnetism, respectively. We also observe a turning point of AFM–FM ordering of Ce^{3+} moment at $x_{c3} \simeq 0.37$. The SC is absent in the phase diagram, which is attributed to the destruction to Cooper pair by Ce-FM fluctuations in the vicinity of x_{c1}. We continue to investigate $CeFeAs_{1-x}P_xO_{0.95}F_{0.05}$. With the separation of x_{c1} and x_{c3}, this chemical pressure results in a broad SC region $0 \leq x \leq 0.53$, while the original HF behavior is driven away by 5% F^- doping. Different roles of P and F dopings are addressed, and the interplay between SC and Ce-4f magnetism is also discussed.

Keywords: superconductivity, iron-based pnictide, Kondo effect, heavy fermion, quantum critical point, chemical pressure effect

PACS: 74.70.Xa, 74.62.Fj, 74.40.Kb, 75.20.Hr **DOI:** 10.1088/1674-1056/22/8/087415

1. Introduction

The discovery of the superconductivity (SC) in the $LaFeAsO_{1-y}F_y$[1,2] triggered extensive interest in search for new high-temperature superconductors.[3–18] Up to now, the highest superconducting transition temperature (T_{sc}) of around 56 K has been achieved in $SmFeAsO_{0.9}F_{0.1}$[7] and $Gd_{0.8}Th_{0.2}FeAsO$.[10] From the viewpoint of crystalline structure, such iron-based pnictides (chalcogenides) are divided into two kinds of space groups: $P4/nmm$ (No. 129) and $I4/mmm$ (No. 139), seeing in Fig. 1. In the former case, two adjacent FeAs(Se) layers stack along the c axis consequently (11 family[14]), and the interstices in between can be intercalated with single atoms (111 family[19]) or atomic clusters (e.g., 1111 family[20] and 21311 family[21]); while in the latter case, the two adjacent FeAs(Se) layers are vertically reversed, and the intercalation by single atoms or atomic clusters forms the families such as 122,[13] 32522,[22] and 43822.[23,24] Besides, there is a hybridization of the two, $La_2Ni_4P_4O_2$,[25] which can be considered as a marriage of $LaNi_2P_2$ and LaNiPO.

As is well known, in the 1111-type pnictide formulated with $LnFePnO$ (Ln = rare earths; Pn = P, As), FeAs(P) layer is a conducting layer, while the LnO layer acts as a carrier reservoir (see Fig. 2(a)). Upon cooling, LnFeAsO undergoes a structural transition from tetragonal phase to orthorhombic phase at T_S,[27] accompanied by an antiferromagnetic (AFM) transition at T_{N1} just below T_S. Such a picture was confirmed by low-temperature X-ray diffraction,[28] ^{57}Fe-Mössbauer spectrum,[29] μ-SR,[28] and ^{139}La-NMR[30] experiments. Yildirim *et al.* considered the LnFeAsO parent compounds on the boundary of correlated Mott insulators,[31–34] and pointed out that in the presence of the magnetic frustration caused by the nearest neighbor exchange and the next nearest neighbor exchange among localized Fe^{2+} moments, neither ferromagnetic (FM) ordering nor checkerboard AFM ordering in LaFeAsO is stable, while the stripe AFM configuration is the only stable ground state. The magnetic stripe phase breaks the tetragonal symmetry, removes the frustration, and causes a structural distortion.

*Project supported by the National Basic Research Program of China (Grant Nos. 2011CBA00103 and 2010CB923003) and the National Natural Science Foundation of China.
†Corresponding author. E-mail: zhuan@zju.edu.cn
© 2013 Chinese Physical Society and IOP Publishing Ltd

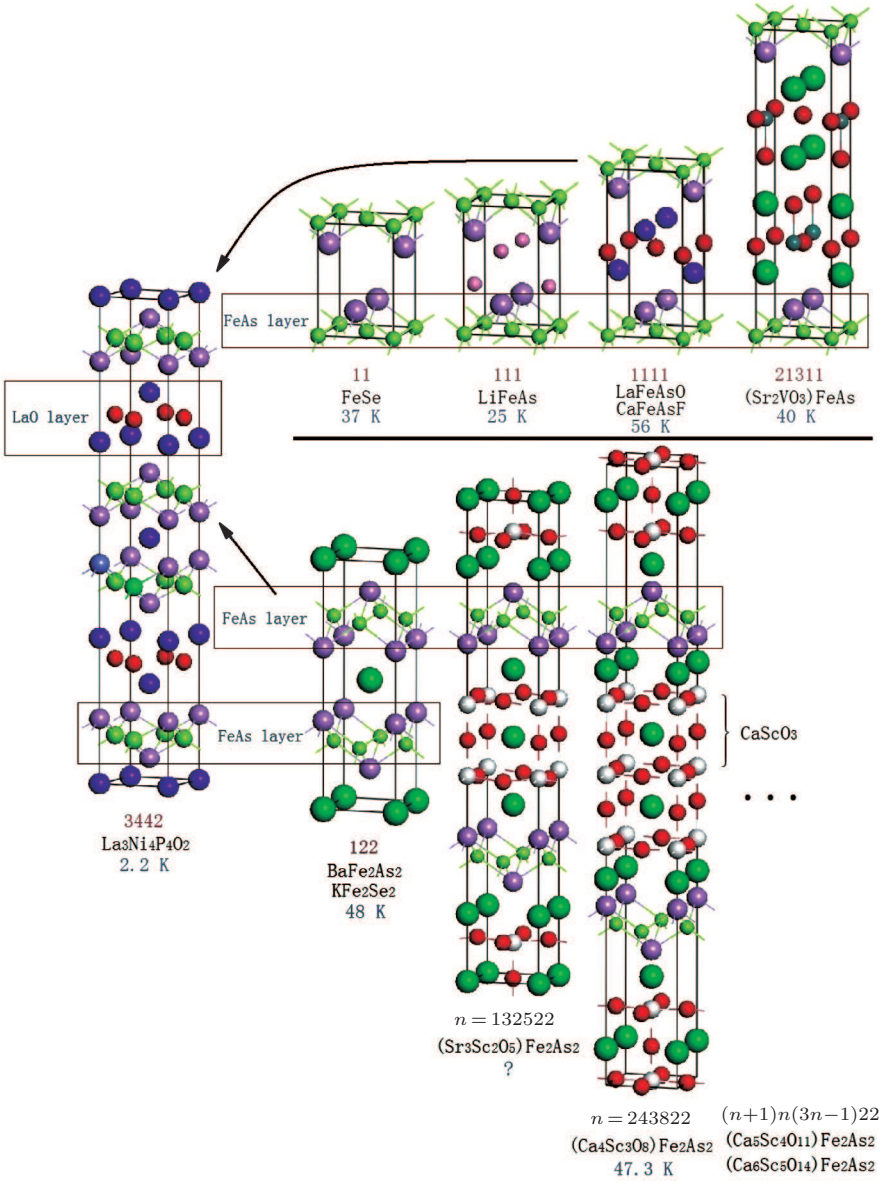


Fig. 1. A global crystalline structure diagram of iron-based pnictides (chalcogenides) and maximal T_{sc} records (under pressure). Data cited from Refs. [13], [14], [19], [21–26].

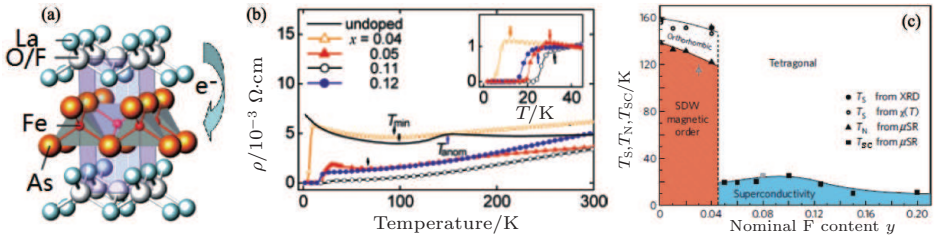


Fig. 2. (a) The crystalline structure of LaFeAsO. (b) SC induced by F^- doping in $LaFeAsO_{1-y}F_y$.[1] (c) Phase diagram of $LaFeAsO_{1-y}F_y$.[37]

Traditionally, there are two ways to achieve SC in iron-based pnictides: chemical doping and pressure effect. Take F^- doping in LaFeAsO for example. Since F adopts one less electron than O to meet with the configuration of $2p^6$, the F^- doping on O^{2-} site "introduces" one extra electron to the FeAs layer. Similar to the high-T_{sc} cuprate superconductor,[35,36] such a chemical doping suppresses the structural distortion and AFM transition, and results in SC at low temperature. Figure 2(b) shows the temperature-dependent resistivity of various F^- concentrated $LaFeAsO_{1-y}F_y$. A representative phase diagram of iron-based pnictide is shown in Fig. 2(c).[37] The phase diagram of pressure effect on iron-based pnictide is more or less analogous to the chemical doping case.[38,39]

Chemical pressure is a special way of chemical doping,

and also a unique kind of pressure. In this context, the chemical pressure means P doping on As site, which is shortened as P/As-doping. Since the ionic radius of P^{3-} (2.12 Å) is less than that of As^{3-} (2.22 Å),[40] this P/As-doping brings about a chemical pressure but meanwhile in principle it does not introduce any extra carrier. Previous first principles calculations on LaFeAsO and LaFePO have elucidated that such a chemical pressure broadens the band structure and thus enhances the itinerancy of carriers, which is also expected for a veritable physical pressure effect.[41] Therefore, this P/As-doping possibly provides a unique controlling parameter to attain a quantum critical point (QCP),[42–44] as shown in Fig. 3(a). The first trial was performed by Wang *et al.*,[45] in which the P/As-doping in LaFeAsO successfully suppresses the Fe-AFM instability and employs SC in the vicinity of the magnetic critical point, as shown in Fig. 3(b). A similar result was also obtained in P-doped $BaFe_2As_2$.[46–48]

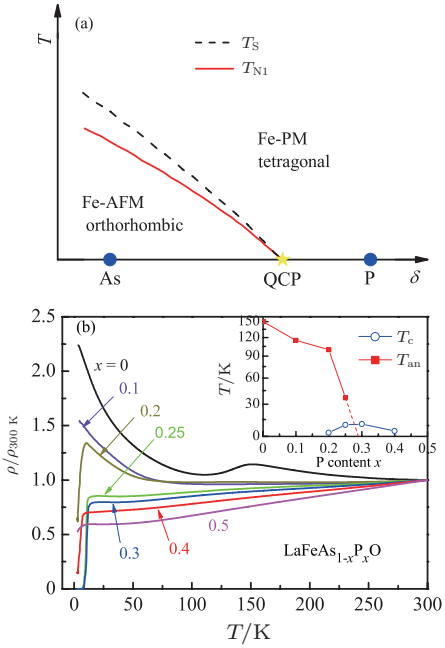


Fig. 3. (a) Theoretically proposed quantum critical point induced by chemical pressure of P/As-doping.[43] (b) SC induced by P doping in $LaFeAs_{1-x}P_xO$. The T_{an} is the anomaly temperature on $\rho(T)$ curve, which roughly characterizes the structural distortion and AFM transition, while T_{sc} is the mid-point of the SC transition.[45]

The current review mainly focuses on the $Ln = Ce$ member of *Ln*FeAsO. Compared with La^{3+}, the additional $4f^1$ electron in Ce^{3+} adds interesting features to CeFeAsO.[49] The compounds Ce*TmPn*O (*Tm* = transition metal) have been confirmed to show a variety of electronic and magnetic properties, depending on the particular *TmPn* layer contained. For instance, CeNiAsO is a correlation-enhanced local-moment antiferromagnet,[50] while CeNiPO behaves as a typical Kondo lattice metal;[51] for the members of *Tm* = Co, both CeCoPO and CeCoAsO show FM correlated Co-3d magnetism.[52–54] In addition, CeOsPO shows Ce^{3+} AFM ordering at 4.5 K, whereas CeRuPO is a rare example of the FM Kondo lattice with $T_C = 15$ K.[55] All these phenomena should be due to the fantasticality of Ce-4f electron. On the one hand, localized magnetic moment emerges in Ce^{3+} and may form long-range magnetism at low temperature. On the other hand, the inter-layer hybridization between Ce and *TmPn* layer furnishes a natural Kondo coupling between Ce-4f moment and conduction electrons. Such a Kondo coupling is expected to be enhanced by P/As-doping chemical pressure, resulting in many peculiar features. We study this chemical pressure effect both in $CeFeAs_{1-x}P_xO$ and $CeFeAs_{1-x}P_xO_{0.95}F_{0.05}$, and investigate the d–f correlation and its influence on SC.

The rest of this review is organized as follows. In Sections 2 and 3, we briefly describe the physical properties of CeFeAsO and CeFePO, respectively. In Section 4, we systematically investigate the phase diagram of $CeFeAs_{1-x}P_xO$, from which two magnetic critical points associated with Fe-AFM ordering and Ce-FM ordering are obtained at $x_{c1} \simeq 0.4$ and $x_{c2} \simeq 0.92$. In addition, we also observe a transition of AFM–FM ordering of Ce^{3+} moments at $x_{c3} \simeq 0.37$. While in the whole phase diagram, we do not observe any trace of SC down to 2 K, which is proposed to be associated with the FM fluctuation in the vicinity of x_{c1}. In Section 5, we continue the research of chemical pressure effect in $CeFeAs_{1-x}P_xO_{0.95}F_{0.05}$, in which 5% F doping leads to $x_{c1} \simeq 0.15$ and $x_{c3} \simeq 0.45$. The separation between x_{c1} and x_{c3} gives rise to robust SC that appears in a wide range of $0 \leq x \leq 0.53$. Meanwhile, x_{c2} is driven out of the phase diagram, leaving $CeFePO_{0.95}F_{0.05}$ an enhanced correlated ferromagnet. In Section 6, we compare this chemical pressure effect with the physical pressure effect on CeFeAsO. Brief summaries and outlooks are presented in Section 7.

2. CeFeAsO: A parent compound of high-T_{sc} superconductor

CeFeAsO, as a parent compound of iron-based pnictide, shares many common features with all the other 1111-type parent compounds. Figure 3(a) shows the temperature dependences of resistivity ($\rho(T)$) of various F^- doped $CeFeAsO_{1-y}F_y$. For CeFeAsO, upon cooling down, $\rho(T)$ increases weakly for $T > 150$ K, in consistence with the bad-metal nature proposed theoretically.[56] At around 150 K, an anomaly is clearly seen on $\rho(T)$ profile. A similar phenomenon was also observed in LaFeAsO and was attributed to a structural distortion accompanied by a spin-density-wave (SDW) type AFM transition.[27] When F^- is doped, this anomaly is substantially suppressed, and superconductivity is achieved. A phase diagram of $CeFeAsO_{1-y}F_y$ was mapped out by Dai *et al.* using neutron scattering technique,[57] as shown in Fig. 4(b). It can follow from the phase diagram that SC appears when F^- is ~6% doped, and reaches optimized doping

at around $y \approx 0.16$ with T_{sc} up to 41 K.[4]

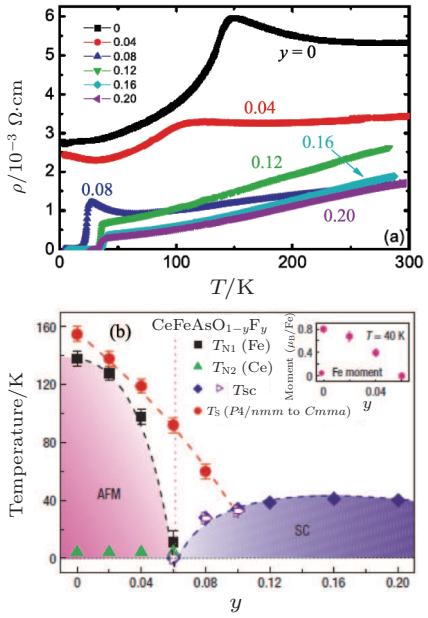


Fig. 4. (a) The temperature dependences of resistivities of $CeFeAsO_{1-y}F_y$.[4] (b) Phase diagram of $CeFeAsO_{1-x}F_x$.[57]

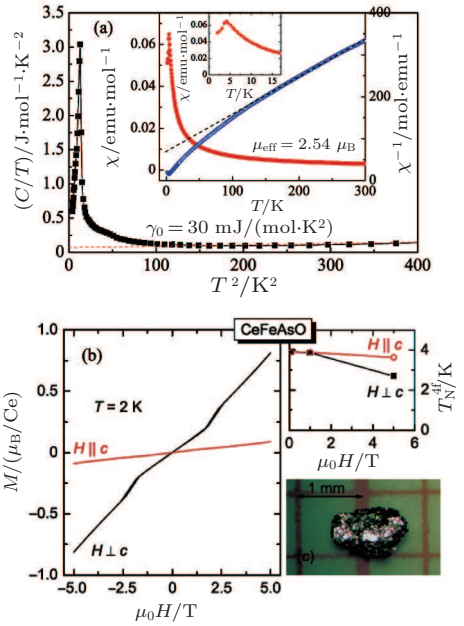


Fig. 5. (a) Plot of specific heat C/T of CeFeAsO versus T^2. Inset shows the temperature dependences of $\chi(T)$ and $1/\chi(T)$. (b) Plots of magnetization of CeFeAsO measured on single crystals.[59]

The difference between CeFeAsO and LaFeAsO comes from the Ce-4f magnetism. In the inset of Fig. 5(a) shown are the plots of dc magnetic susceptibility of CeFeAsO versus T. The $\chi(T)$ conforms to Curie–Weiss's law for T above 150 K, with the effective moment $\mu_{\rm eff} = 2.54\ \mu_{\rm B}$, close to that of a free Ce^{3+} ion. The Ce^{3+} moments form long-range AFM ordering at low temperature, which is determined by the prominent λ-shaped peak at around $T_{\rm N2} = 4.2$ K (see Fig. 5(a)). The Sommerfeld coefficient of CeFeAsO is $\gamma_0 = 30$ mJ/(mol·K^2), which is 20 times larger than that of LaFeAsO (1.405 mJ/(mol·K^2)),[58] indicative of relatively weak correlation between d and f electrons. Furthermore, magnetization measurement on single crystalline CeFeAsO shows highly anisotropic magnetism, with *ab* plane being the magnetically easy plane (see Fig. 5(b)).[59] In addition, there is a field-induced spin-flop metamagnetic transition at around 2.0 T for $T < T_{\rm N2}$. All these above demonstrate that CeFeAsO is embedded in a long-range AFM regime with Ce-4f electrons well localized, and meanwhile the Kondo effect is weak.

3. CeFePO: A heavy fermion metal with FM correlations

Turning now to the phosphorus end compound CeFePO.[60] Figure 5(a) shows temperature-dependent specific heat C/T curves under various fields. It is clearly seen that $C^{\rm 4f}/T$ ($C^{\rm 4f}$ was derived by subtracting the specific heat of LaFePO[61]) increases logarithmically with temperature decreasing below 10 K and becomes saturated below 2 K at $\gamma_0 = 700$ mJ/(mol·K^2). This magnitude of Sommerfeld coefficient has been greatly enhanced, compared with that of LaFePO (12.5 mJ/(mol·K^2)), manifesting the intensive contribution from renormalized narrow bands. The resistivity $\rho(T)$ initially decreases almost linearly via cooling down from room temperature, before it drops rapidly below 30 K due to the onset of coherent Kondo scattering (see the upper inset of Fig. 6(a)). Below $T = 1$ K, $\rho(T)$ follows a $\rho \propto T^2$ dependence, indicating that the formation of a Landau–Fermi liquid ground state is consistent with the specific heat (see the lower inset of Fig. 6(a)). Figure 6(b) shows ^{31}P field-sweep NMR spectra measured at various temperatures and $\nu = 76.4$ MHz. One single narrow ^{31}P NMR line as expected from the crystalline structure was found at room temperature (see the right panel in Fig. 6(b)). It develops strong anisotropy towards lower temperatures (see the left panel in Fig. 6(b)). The broadened ^{31}P NMR lines could be simulated, and they are in consistence with shift-tensor components $K_{\rm ab}(T)$ and $K_{\rm c}(T)$ (corresponding to the $\boldsymbol{H} \perp \boldsymbol{c}$ and $\boldsymbol{H} \parallel \boldsymbol{c}$, respectively) at all temperatures (see the inset in Fig. 6(b)). While $^{31}K_{\rm c}(T)$ is almost independent of T, $^{31}K_{\rm ab}(T)$ increases significantly with decreasing temperature (see Fig. 7(a)). Above 15 K, $^{31}K_{\rm iso} \equiv 2K_{\rm ab}/3 + K_{\rm c}/3$ tracks the bulk susceptibility $\chi(T)$ obtained by MPMS measurements at 5 T (see the lower inset of Fig. 7(a)). Below 10 K, the line shape of the spectrum

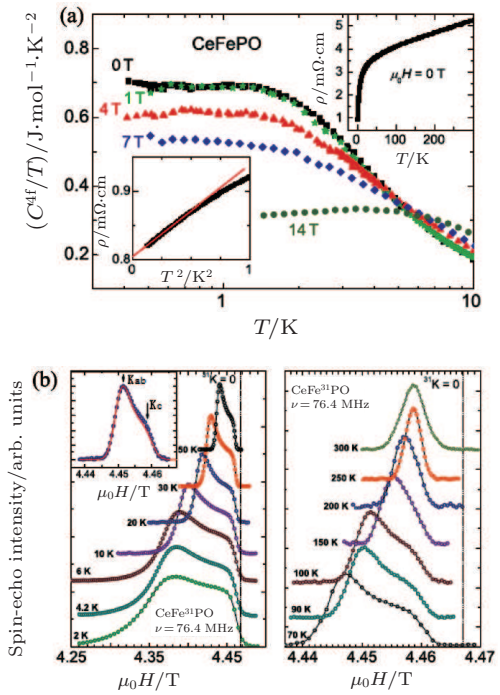


Fig. 6. (a) Specific heat C/T versus T under various fields. The insets show $\rho(T)$. (b) ^{31}P field-sweep NMR spectra at $\nu = 76.4$ MHz and different temperatures.[60]

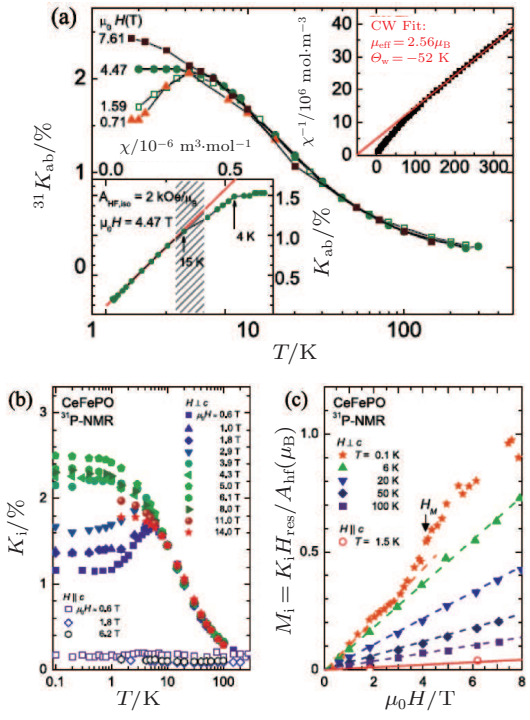


Fig. 7. (a) Plots of shift component $^{31}K_{ab}$ versus T in different magnetic fields.[60] (b) Temperature dependence of the Knight shift determined at the peaks of $\boldsymbol{H} \perp \boldsymbol{c}$ and $\boldsymbol{H} \parallel \boldsymbol{c}$ spectra obtained at various H. (c) H dependence of magnetization M for $\boldsymbol{H} \perp \boldsymbol{c}$ and $\boldsymbol{H} \parallel \boldsymbol{c}$.[62]

becomes field-dependent. While at high fields ($\mu_0 H > 7$ T), the line shape observed at higher temperatures is maintained down to 2 K. Reducing the field to below 4 T leads to both a strong broadening of the contribution related to $\boldsymbol{H} \perp \boldsymbol{c}$ and a shift of its maximum towards lower T values. In contrast, the contribution connected with $\boldsymbol{H} \parallel \boldsymbol{c}$ is not affected. Such a broadening is typical for the onset of short-range FM correlations. At high fields, $K_{ab}(T)$ increases to the lowest T, while at low fields it forms a clear maximum at around 4 K. This specific field dependence also appears to suggest that CeFePO is close to an FM instability (see Fig. 6(a)). All these above indicate that CeFePO is an HF metal with FM correlations. In 2012, Kitagawa *et al.* systematically investigated the ^{31}P NMR spectra[62] on bulk single crystals, and reported that CeFePO with two-dimensional XY-type anisotropy shows a metamagnetic-like behavior at $H_M \simeq 4$ T perpendicular to the c axis and that a critical behavior is observed around H_M, as shown in Fig. 7(c). Such a metamagnetic-like behavior is reminiscent of a field-induced delocalized–localized transition approaching to the critical point which is a signature of Kondo breakdown.[62–64] These observations possibly put CeFePO on a boundary of an exotic FM QCP.[65] Therefore, it will be of great interest to study the phase diagram of $CeFeAs_{1-x}P_xO$.

4. The two magnetic critical points in $CeFeAs_{1-x}P_xO$

The powder X-ray diffraction (XRD) patterns of the $CeFeAs_{1-x}P_xO$ are shown in Fig. 8. All the XRD peaks can be well indexed based on the tetragonal ZrCuSiAs-type structure with the space group $P4/nmm$ (No. 129), and no obvious impurity phases can be detected, suggesting high quality of the samples. As shown in Figs. 8(a) and 8(b), all the XRD peaks shift towards the right-hand side, especially for the high angle reflections. Upon P doping, the (003) peak shifts much faster than the (110) peak so that the former catches up with the latter at around $x = 0.6$. For higher P concentration $x > 0.6$, the two peaks merge together. This observation demonstrates that the c axis shrinks much faster than the a axis, which is consistent with the calculated lattice parameter shown in Fig. 8(c). For comparison, the refined structural parameters of CeFeAsO and CeFePO are summarized in Table 7. The remarkable difference in structure lies in the positions of Ce and As/P. For CeFePO, the thickness of FeP layer is much smaller, and meanwhile, Ce atomic layers are much closer to the FeP layers. This structural feature supports the increasing coupling between Fe-3d and Ce-4f electrons as P dopes. All these show that the P doping on As site acts as a "chemical pressure" effect.[43] In the following part, we will systematically describe the effects of this chemical pressure on the electronic and magnetic properties of CeFeAsO.

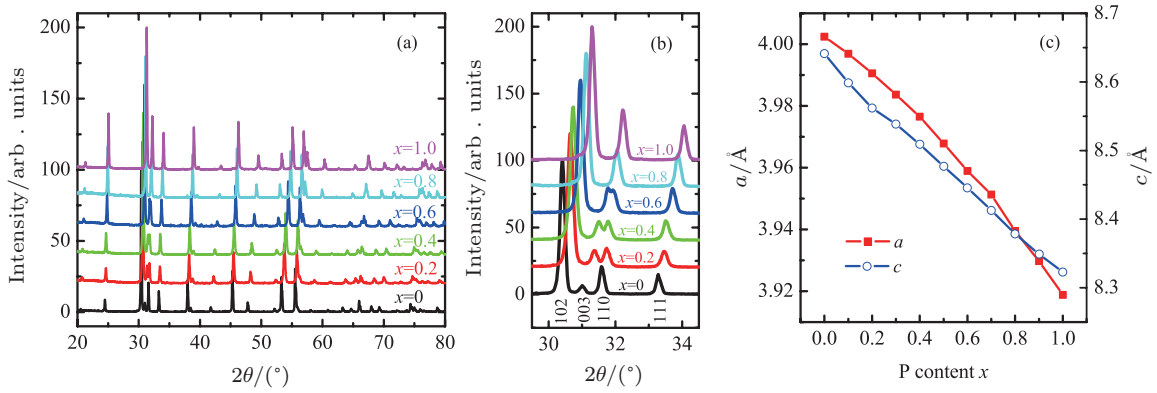


Fig. 8. (a) XRD patterns of $CeFeAs_{1-x}P_xO$. (b) Enlarged plots of (a). (c) Plots of lattice parameters a and c versus P doping concentration x.[66]

Table 1. Comparison of lattice parameters between CeFeAsO and CeFePO. Results from Rietveld refinement. Atomic positions: Ce (1/4, 1/4, z_{Ce}), Fe (3/4, 1/4, 1/2), *Pn* (1/4, 1/4, z_{Pn}), O (3/4, 1/4, 0).

CeNi*Pn*O	CeFeAsO	CeFePO
a/Å	4.0024	3.9189
c/Å	8.6412	8.3228
z_{Ce}	0.1415	0.1506
z_{Pn}	0.6556	0.6437
d_{FePn}/Å	2.4109	2.2956
$\theta_{Pn-Fe-Pn}$/(°)	112.21	117.20
R_{wp}	11.96%	11.91%
R_p	8.16%	7.77%
χ^2	1.12	1.14

The temperature-dependent resistivities of $CeFeAs_{1-x}P_xO$ are shown in Fig. 9, from which five prominent features can be identified. (i) The conductivity of $CeFeAs_{1-x}P_xO$ has been greatly enhanced from CeFeAsO to CeFePO, for example, the resistivity of CeFeAsO at $T = 300$ K is $\rho(300\ \mathrm{K}) = 300$ μΩ·m, while for CeFePO, it reduces to only 12 μΩ·m, indicating that P doping enhances the metallicity significantly. Such a trend of P doping is consistent with that of chemical pressure which broadens the bandwidth.[41,67] (ii) The resistivity anomaly. Such an anomaly is mostly prominent for $x = 0$, and is ascribed to the structural distortion and the accompanied Fe–AFM transition.[57,68] Upon doping, the anomaly is suppressed monotonically and soon becomes an unremarkable kink at lower temperatures. No clear kink can be identified for $x > 0.3$. The suppression of this anomaly with P doping is consistent with that of AFM ordering of Fe ions, which was confirmed by neutron study.[69] We mark arrows in Fig. 9(a) to show the Fe-AFM transition (T_{N1}).[69] (iii) The resistivity upturns at low temperatures for $x \leq 0.4$. The upturn behavior is suppressed by doping or magnetic field (see the inset in Fig. 9(b)), indicating that the Ce-AFM moment polarizes under external field and thus reduces spin scattering. (iv) For $x > 0.4$, $\rho(T)$ undergoes an inflection below 20 K before dropping rapidly. We will find that this inflection is a precursor of the Ce-FM ordering that will reduce the spin-flip scattering. (v) For even larger x close to the CeFePO end, the inflection disappears and is replaced by a round downturn, signalizing the onset of Kondo coherence. However, no SC is observed down to $T = 2$ K for the entire P doping range. It should be noticed that the transition temperatures of the Fe-AFM ordering and the structural distortion can be approximately determined from the resistivity anomaly (see Fig. 9) and neutron studies (see Fig. 10).[69] They are undistinguishable in resistivity when $x > 0.2$. The neutron study[69] revealed that both of them are suppressed and terminate at $x_{c1} \sim 0.4$.

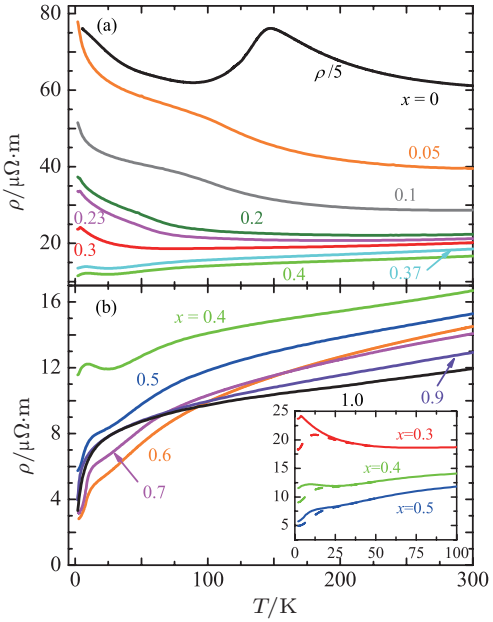


Fig. 9. Temperature dependences of resistivity $\rho(T)$ of $CeFeAs_{1-x}P_xO$ for (a) $0 \leq x \leq 0.4$ and (b) $0.4 \leq x \leq 1$. Inset of (b) shows the curves of $\rho(T)$ under $\mu_0 H = 0$ (solid lines) and 5 T (dashed lines).[66]

Figure 10 shows the temperature dependences of structural and Fe magnetic Bragg peaks for various P concentrations, which are obtained by neutron scattering experiment.[69] As the crystal structure changes from the tetragonal phase at high temperature to the orthorhombic phase at low temperature, the $(2, 2, 0)_T$ peak will split into two peaks,[27] and a sudden reduction in the scattering intensity at the $(2, 2, 0)_T$ peak position reveals the transition temperature for the lattice distortion (see Fig. 10(a)). With the increase in phospho-

rus concentration, the tetragonal-to-orthorhombic lattice distortion transition temperature T_S decreases gradually, while it is hard to identify the structural phase transition temperatures (if any) for $x > 0.3$. It follows from T_S that the Fe ion magnetic ordering seems to be suppressed by P doping more continuously, see Fig. 10(b), which is reminiscent of the possibility of a magnetic quantum critical point[43] at $x_{c1} \sim 0.4$.

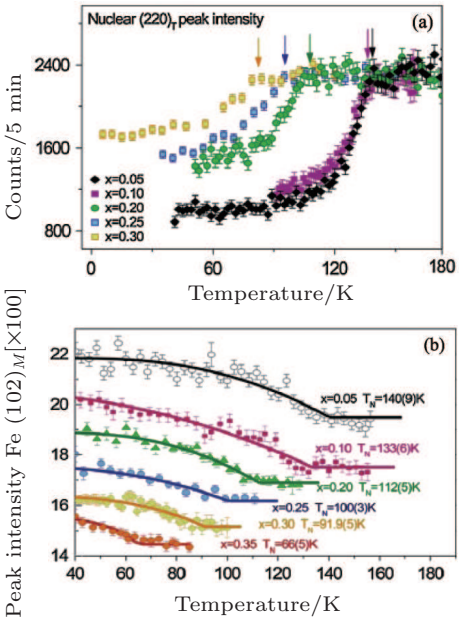


Fig. 10. (a) Temperature dependences of the $(2, 2, 0)_T$ Bragg peak intensity for different samples, which shows clear kinks indicative of tetragonal-to-orthorhombic phase transitions. (b) Temperature dependences of the order parameter at the Fe magnetic Bragg peak position $(1, 0, 2)_M$ as a function of P concentration. The solid lines represent mean field fitting to the data.[69]

The temperature dependences of dc magnetic susceptibilities are shown in Fig. 11. For all the samples $0 \leq x \leq 1$, $\chi(T)$ obeys Curie–Weiss's law at $T > 150$ K. We fit susceptibility to the formula $\chi(T) = \chi_0 + C/(T - \theta_W)$, where χ_0 is the temperature-independent item and θ_W is the Weiss temperature. The values of derived effective moment μ_{eff} are 2.54 μ_B for $x = 0$ and 2.56 μ_B for $x = 1$ (see insets in Fig. 11), very close to that of a free Ce^{3+} ion, 2.54 μ_B. This means that Ce-4f electrons are well localized in this regime, which is consistent with the fact that $T_K \sim 10$ K for CeFePO. By lowering temperatures, a clear peak is observed at 4.16 K for $x = 0$, which is related to the formation of the Ce^{3+} AFM ordering. With the increase in x, $\chi(T)$ increases and the peak becomes round (or shoulder-like); whereas the corresponding AFM ordering temperature does not change too much. For $x > 0.4$, an obvious discrepancy between zero-field cooling (ZFC) and field cooling (FC) is seen at lower temperatures (see Fig. 11(b)), manifesting the FM ordered ground state of the Ce-4f moment. The suppression of AFM and development of FM are consistent with the enhanced metallicity in the process of P doping. The FM ordered state persists until $x \sim 0.9$, where the divergency of $\chi(T)$ vanishes. We should also emphasize that the magnitude of $\chi(T)$ also decreases for $x > 0.9$, indicating that FM ordering dies away.

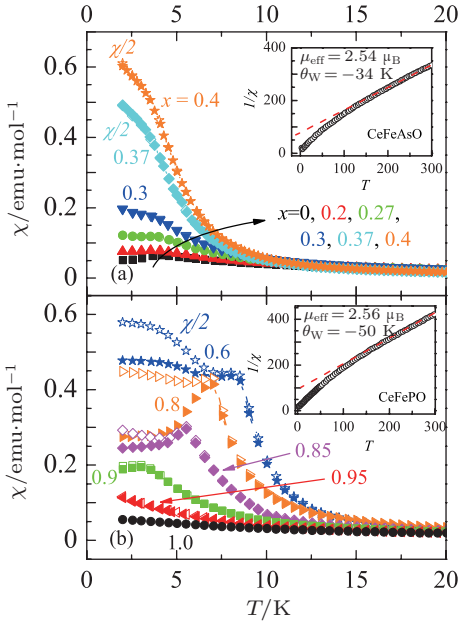


Fig. 11. Temperature dependences of magnetic susceptibility $\chi(T)$ of $CeFeAs_{1-x}P_xO$ measured under $H = 1000$ Oe for (a) $0 \leq x \leq 0.4$ and (b) $0.4 < x \leq 1$. Insets of (a) and (b) display Curie–Weiss behaviors of $1/\chi$ for CeFeAsO and CeFePO, respectively.[66]

The evolution of Ce^{3+} magnetism can be further demonstrated by isothermal field dependent magnetization measurements, which are shown in Fig. 12. The temperatures are fixed to be 2 K (solid line) and 10 K (dashed line), respectively. For $x = 0$ and $T = 2$ K, a kink in the magnetization curve is clearly seen, indicating a possible field-induced spin flop transition in the AFM state of Ce^{3+} moment, compatible with Jesche *et al.*'s measurement on single crystal.[59] As x increases, the kink vanishes. As $x \geq 0.4$, $M(H)$ starts to increase rapidly for low fields and tends to be saturated at higher fields, i.e., it exhibits a nonlinear field dependence for $x = 0.4$ (see Fig. 12(d)). For $0.5 < x < 0.9$, clear hysteresis loops can be observed at 2 K and the saturated M value reaches the maximum around $x = 0.6$ (see Fig. 12(e)). Therefore, the long-range FM ordering is established in a wide doping range between $x \sim 0.4$ and $x \sim 0.9$. The largest saturated magnetic moment is about 0.95 μ_B/Ce, close to 1 μ_B/Ce which is expected for a Ce^{3+} doublet ground state.[60,70] For $0.9 < x < 0.95$ the hysteresis loop is hardly resolvable down to the lowest measured temperature, while the saturation tendency persists. This may be due to strong FM fluctuations at the quantum critical point associated with the 4f electrons. On the other hand, both the susceptibility and magnetization show a non-magnetic HF-like phase for $x \geq 0.95$ (see Figs. 11(b) and 12(g)–12(h)), which is consistent with the resistivity measurement.

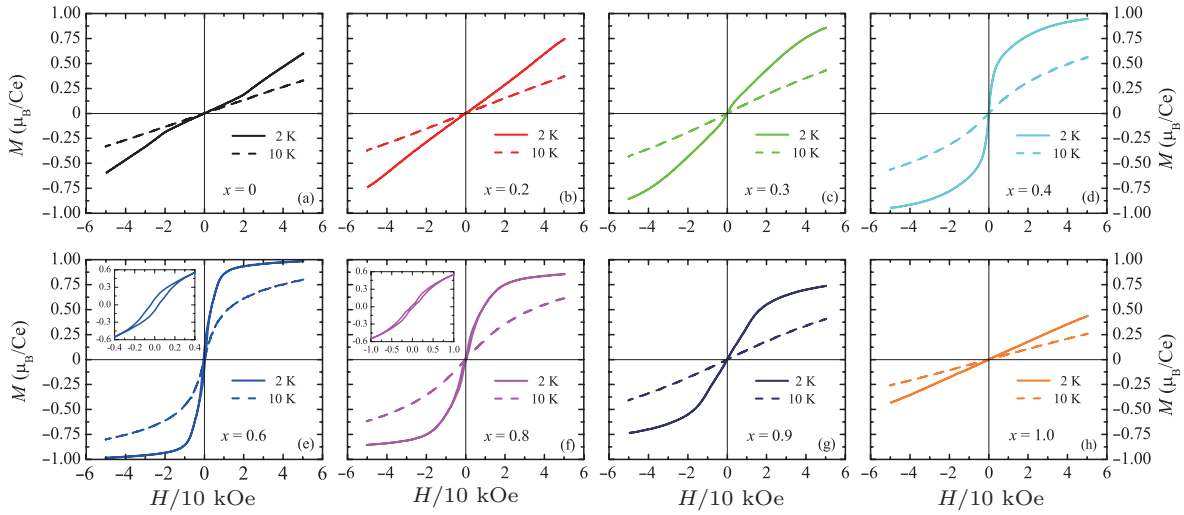


Fig. 12. Curves of isothermal magnetization $M(H)$ of $CeFeAs_{1-x}P_xO$, measured at 2 K (solid line) and 10 K (dashed line) at (a) x =0, (b) 0.2, (c) 0.3, (d) 0.4, (e) 0.6, (f) 0.8, (g) 0.9, and (h) 1.0. Insets of panels (e) and (f) show hysteresis loops.[66] The unit 1 Oe = 79.5775 A·m^{-1}.

The metallic HF-like behavior can be further manifested by the specific heat measurement as shown in Fig. 13. For $x = 0.95, 0.97$, and 1, the specific heat coefficient $C(T)/T$ shows $-\log T$ behavior at low temperatures down to 2 K, manifesting non-Fermi-liquid (NFL) behavior. According to previous work reported by Brüning *et al.*,[60] for $x = 1$, C/T is saturated below 1 K and results in a large Sommerfeld coefficient $\gamma_0 = 700$ mJ/(mol·K^2), in agreement with our results. We define a characteristic temperature T_γ (well below which HF-like behavior is deeply established) as the intersection of two extrapolate lines of the specific heat data as shown in the inset of Fig. 13. For the $x = 1$ sample, $T_\gamma \sim 8.6$ K. As a comparison, $\gamma(T)$ shows a λ-shaped peak positioned at ~ 4.2 and 6.8 K for both $x = 0$ and 0.8, in the AFM and FM ordered phases, respectively. A sudden increase in saturated γ_0 close to $x \sim 0.9$ can be inferred by the value of C/T at $T = 2$ K, accompanied by a decrease in the saturated magnetization under $\mu_0 H = 5$ T. This implies the enhancement of the Kondo screening near the FM instability. It should be noted that a very tiny kink is observed around 6 K on the C/T versus T curve of $x = 0.95$. We ascribe this additional peak to the tiny magnetic impurity Ce_2O_3 which undergoes an AFM transition at 5.7 K.[71]

An electronic phase diagram is shown in Fig. 14(a). At low temperatures, both the Fe-3d and Ce-4f electrons show the long-range AFM ordering for $x \leq 0.37$. The d electrons are Pauli paramagnetic (PM) for $x \geq 0.4$, while the f electrons are FM ordered until $x \sim 0.9$. For $x \geq 0.95$, the f moments are completely quenched and the whole system becomes a non-magnetic HF-like metal. The HF-like region is roughly depicted by T_γ (note that strictly speaking, T_{FL}, below which Landau's Fermi liquid develops, should be much lower than T_γ[60]). Therefore, in addition to the first magnetic critical point (denoted by x_{c1}) associated with the AFM–PM transitions of the 3d electrons, there could be another magnetic critical point associated with the FM–HF transition of 4f electrons around $x = 0.92$ (denoted by x_{c2}). The value of x_{c1} has been known to be $\sim$0.4 by neutron scattering experiment.[69] The turning point (denoted by x_{c3}) associated with the AFM–FM transition of the 4f electrons at $x_{c3} \simeq 0.37$ is quite close to x_{c1}. Meanwhile, strong FM fluctuation shows up in the vicinity of x_{c2}.

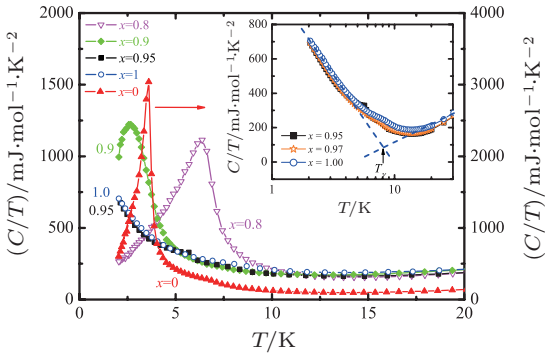


Fig. 13. Plots of specific heat C/T of $CeFeAs_{1-x}P_xO$ versus T. The inset shows the NFL behavior for $x \geq 0.95$.[66]

First, as the suppression of the a axis is only a fraction of that of the c axis upon P doping, the electronic states in the Ce–O layer should not change significantly. This is also supported by the non-magnetic LDA calculation in which the difference between Fermi surfaces of CeFeAsO and CeFePO can be mainly ascribed to the pnictogen height.[41,44] Therefore, the HF behavior in the end compound, CeFePO, originates apparently from the inter-layer coupling between the Fe-3d and Ce-4f electrons. Second, the AFM–FM transition associated with Ce^{3+} moment could be explained by assuming the existence of a bare d–f Kondo coupling (J_0) in the ordered phases, as

it can modulate the indirect Ruderman–Kittel–Kasuya–Yosida (RKKY) interaction (J_{RKKY}) between the Ce-4f local moments. Intuitively, the exchange interaction between the local 4f moments, J_f, is given by $J_f = J_f^{(0)} + J_{RKKY}$, with $J_f^{(0)} < 0$ being the exchange interaction bridged by O or As/P atoms in the absence of J_0,[72–74] and $|J_{RKKY}| \sim J_0^2 N(\varepsilon_F)$,[75–77] with $N(\varepsilon_F)$ being the density of states (DOS) at Fermi level (of mainly d-electron characteristic). The value of J_f is negative if $J_0 N(\varepsilon_F)$ is small, as it should be, since the parent compound CeFeAsO is a bad metal and shows an AFM transition.[4,78,79] Upon P doping, both J_0 and $N(\varepsilon_F)$ increase, leading to a sign change in J_f. Third, the monotonic increase in $J_0 N(\varepsilon_F)$ is also the driving force for the quench of Ce-4f magnetism around x_{c2}, where the Kondo scale T_K, which increases exponentially with $J_0 N(\varepsilon_F)$,[80] starts to dominate over the magnetic ordering energy scale, $T_f \approx |J_f|$. Herein, we propose an extended Doniach picture[80,81] as shown in the inset of Fig. 14(a), which qualitatively describes the observed AFM–FM–HF evolution of the 4f-electron ground state in $CeFeAs_{1-x}P_xO$. Finally, it is of great interest to make a comparison with $LaFeAs_{1-x}P_xO$ in which SC is induced by this chemical pressure.[45] We attribute this absence of SC in $CeFeAs_{1-x}P_xO$ to the Ce-FM ordering in the vicinity of x_{c1}. More evidences will be derived in the case $CeFeAs_{1-x}P_xO_{0.95}F_{0.05}$ discussed in next section.

It is also necessary to discuss the possibilities of QCPs for x_{c1} and x_{c2}. The chemical pressure induced QCP has been identified in $BaFe_2(As_{1-x}P_x)_2$.[46–48] The Fe-AFM ordering is continuously suppressed by P/As-doping at $x_{c1} = 0.33$, and SC with maximal $T_{sc} = 30$ K was achieved in the vicinity of the critical point. Furthermore, NFL behaviors with low power law of $\Delta\rho(T)$ and strong AFM fluctuations were observed near x_{c1}. All these are suggestive to a QCP phenomenon in $BaFe_2(As_{1-x}P_x)_2$. However, to the best of our knowledge, in the case of 1111-type pnictides such as $LaFeAs_{1-x}P_x$ and $CeFeAs_{1-x}P_x$, no direct evidence has been derived to support the continuity of Fe-AFM suppressed by chemical pressure, nor was the NFL behavior confirmed around x_{c1}. Therefore, it might be too arbitrary to call it a QCP right now. On the other hand, x_{c2} seems to be more promising, because of the NFL and HF behavior observed near x_{c2} and the FL metallicity above it.[60] Further investigation is required to clarify these issues in the future.

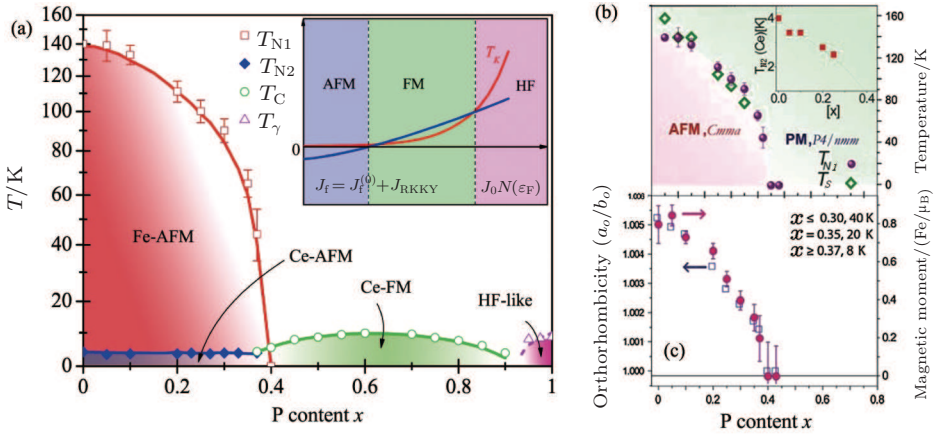


Fig. 14. (a) Electronic phase diagram of $CeFeAs_{1-x}P_xO$.[66] (b) The phase diagram determined by neutron scattering technique. (c) P-doping dependence of the orthorhombicity and Fe ordered moments.[69]

5. Interplay of the SC and Ce-magnetism in $CeFeAs_{1-x}P_xO_{0.95}F_{0.05}$

Figure 15 shows the XRD patterns of six representative samples of $CeFeAs_{1-x}P_xO_{0.95}F_{0.05}$. All the samples are of high purity while no obvious impurities phases can be detected. All the diffraction peaks can be well indexed based on the $P4/nmm$ (No. 129) space group with tetragonal ZrCuSiAs-type structure, ensuring the high quality of these samples. Similar to the case of $CeFeAs_{1-x}P_xO$,[66] all the peaks shift rightward with P content increasing, indicating the shrinkage of both lattice constants a and c. It is also found that the c axis decreases faster than the a axis, as shown in the inset of Fig. 15. It is very interesting that the F doping, in the two end compounds, CeFeAsO and CeFeAsP, causes opposite changes in lattice parameters. In CeFeAsO, both a and c axes decrease due to F doping, while in CeFePO, on the contrary, both a and c axes increase. A similar phenomenon was also observed in $LaFePO_{1-y}F_y$,[83] and will be discussed later.

The temperature dependences of resistivity are shown in Figs. 16(a) and 16(b) for all $CeFeAs_{1-x}P_xO_{0.95}F_{0.05}$ ($0 \leq x \leq 1$) samples. Three prominent features can be identified in the profiles of resistivity. i) The resistivity decreases almost linearly with decreasing temperature for all the samples at temperatures above 100 K, confirming the metallicity of F-doped

$CeFeAs_{1-x}P_xO$. ii) In the underdoped regime ($x < 0.15$), there is a clear upturn in the $\rho(T)$ curve at low temperatures. Upon P doping, the upturn is suppressed to lower temperatures, and vanishes at the over-doped regime ($x > 0.15$). This P-doping-dependent upturn could be associated with the residual structural distortion and/or AFM transition of Fe-3d electrons. Actually, according to the phase diagram mapped by the neutron scattering on $CeFeAsO_{1-y}F_y$,[57] the AFM instability of 3d electrons persists until 6% F doping, and the structural distortion survives to even higher F^- concentration. Thus, it is reasonable to claim that these phase transitions could still exist in the $CeFeAs_{1-x}P_xO_{0.95}F_{0.05}$ system. For a spin fluctuation mediated SC, the highest T_{sc} usually emerges at the point where the AFM ordering is totally suppressed. From this perspective, we may estimate that $x_{c1} \sim 0.15$ in $CeFeAs_{1-x}P_xO_{0.95}F_{0.05}$. iii) No SC is observed down to the lowest measured temperature 2 K for $x \geq 0.55$ and there is a broad hump around 70 K–100 K for all the samples in this region. Such a hump could be reminiscent of crystalline electric field (CEF) effect.[70]

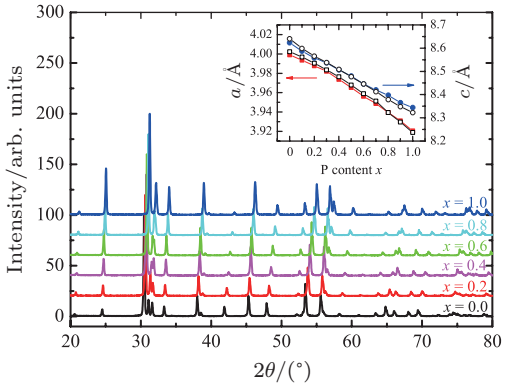


Fig. 15. XRD patterns of $CeFeAs_{1-x}P_xO_{0.95}F_{0.05}$. Inset shows lattice parameters a and c versus P doping concentration x. The open symbols denote $CeFeAs_{1-x}P_xO$, while the solid ones represent $CeFeAs_{1-x}P_xO_{0.95}F_{0.05}$.[82]

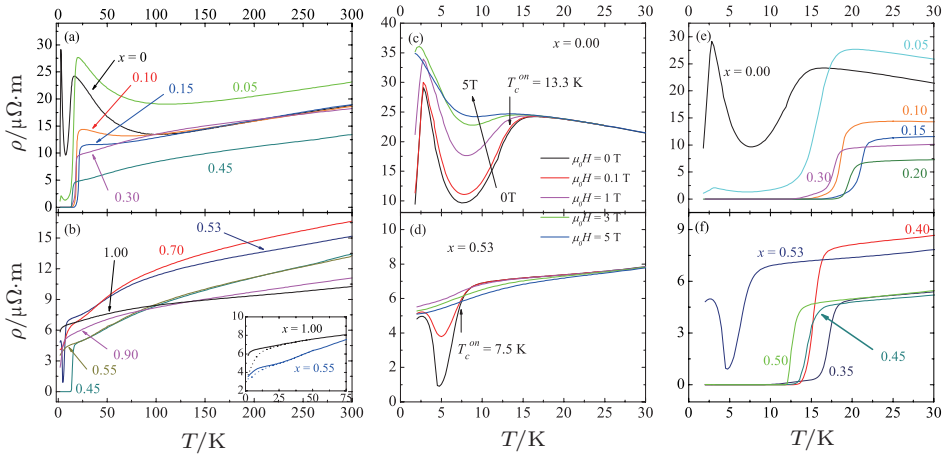


Fig. 16. Plots of resistivity versus T of $CeFeAs_{1-x}P_xO_{0.95}F_{0.05}$ for (a) $0 \leq x \leq 0.45$ and (b) $0.45 \leq x \leq 1$, respectively. The inset in panel (b) shows the curves of $\rho(T)$ of $x = 0.55$ and 1.0 under $\mu_0 H = 0$ (solid line) and 5 T (dashed line). Panels (c) and (d) display the SC re-entrances of $x = 0$ and 0.53, respectively. Panels (e) and (f) show SC transitions for $x \leq 0.53$.[82]

Now we focus on the resistivity profiles for $0 \leq x \leq 0.53$, i.e., the SC regime, presented in Figs. 16(c)–16(f). For $x = 0$, $CeFeAsO_{0.95}F_{0.05}$ is on the verge of the SC regime. As temperature is lowered down from room temperature, $\rho(T)$ decreases almost linearly until 100 K where an upturn occurs. As temperature further drops, there is a sharp decrease around 13.3 K, followed by a distinct peak at 2.8 K. The latter is reminiscent of Ce-4f AFM transition as in the parent compound CeFeAsO,[59] which will be further confirmed by temperature dependence of susceptibility whereafter (see Fig. 17(a)). The drop around 13.3 K is a superconducting transition which is confirmed by the magnetization measurement shown in Fig. 17(a). When the magnetic field increases (see Fig. 16(c)), the resistivity drop becomes less prominent, the SC transition becomes broader, and the onset transition temperature T_{sc}^{on} (defined as the temperature at which resistivity drops to 90% of the normal state) is suppressed to a lower temperature. Upon P doping, the SC transition becomes much more obvious, and T_{sc}^{on} increases to 17.4 K for $x = 0.05$, but still no zero resistance is reached. This is due to the re-entrance caused by Ce^{3+} AFM ordering. When P content is further increased, i.e., $x \geq 0.1$, a genuine SC is obtained, and T_{sc}^{on} reaches a maximum of 21.3 K for $x = 0.15$. The decrease in T_{sc}^{on} begins as $x > 0.15$. To see the SC transition clearly, the enlarged plot of resistivity for $CeFeAs_{1-x}P_xO_{0.95}F_{0.05}$ ($0 \leq x \leq 0.53$) is shown together in Figs. 15(e) and 15(f). The SC persists up to $x = 0.53$, and again there is an emergent re-entrance around 5 K (see Fig. 16(d)). The magnetoresistance measurement confirms the SC transition with $T_{sc}^{on} = 7.5$ K. However, when the applied magnetic field is strong enough ($\mu_0 H > 1$ T), SC is completely suppressed, and the magnetoresistance of normal state becomes negative, indicating an intrinsic FM state of Ce-4f correlation. This FM feature will be discussed later on. To the best of our knowledge, it is the first example that both AFM and FM

orderings of 4f-magnetism coexist with SC in 1111-type pnictides. It should be pointed out that all these results are reproducible on different samples with the same composition. We should also emphasize that an SC re-entrance caused by AFM ordering is quite rare, and the mechanism is still unknown. One possibility is that the Ce^{3+} moments are canted and have some FM component in a specific direction.

The SC of the $CeFeAs_{1-x}P_xO_{0.95}F_{0.05}$ ($0 \leq x \leq 0.53$) samples is also confirmed by the temperature-dependent dc magnetic susceptibility measured under $H = 10$ Oe, as shown in Figs. 17(a) and 17(b). For $x = 0$, no bulk Meissner diamagnetic effect can be observed, but only a kink is visible near the transition temperature on the $\chi(T)$ curve. Upon P doping, Meissner diamagnetic effect becomes more obvious, and the volume fraction of magnetic shielding reaches over 70% for the optimal P doping case, $x = 0.15$. While for $x = 0.53$, on the right boundary of the SC regime, no drop in susceptibility due to the SC transition is observed. Instead, a divergency between the ZFC and FC measurements caused by the Ce-4f FM ordering (see below) can be found. As $x > 0.53$, no SC can be identified in either resistivity or susceptibility down to 2 K. For the optimally doped sample ($x = 0.15$), we further measure magnetic susceptibility under different magnetic fields, to manifest the homogeneity of coexisting SC and Ce-4f magnetism, see the inset of Fig. 17(c).

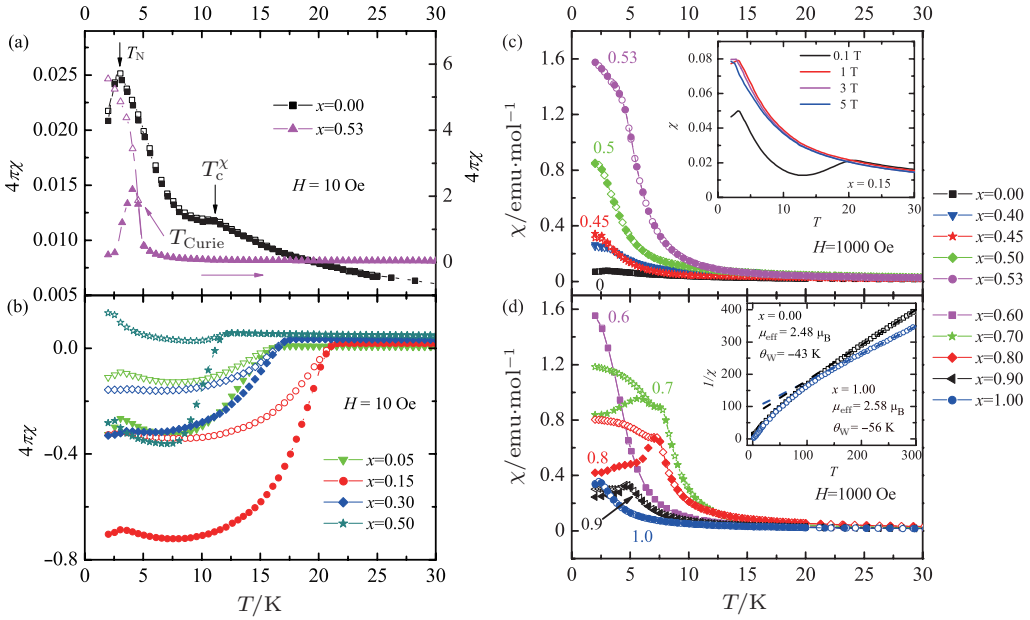


Fig. 17. Temperature-dependent magnetic susceptibilities of $CeFeAs_{1-x}P_xO_{0.95}F_{0.05}$. Solid symbols are for ZFC while open ones for FC. (a) $\chi(T)$ of $x = 0$ and 0.53, $H = 10$ Oe; (b) $x = 0.05$, 0.15, 0.30, and 0.50, $H = 10$ Oe; (c)–(d), $\chi(T)$ curves measured under $H = 1000$ Oe. The inset of panel (c) shows the curves of $\chi(T)$ of $x = 0.15$ under various fields. The inset of panel (d) shows Curie–Weiss behaviors of $1/\chi$ for $x = 0.00$ and 1.00.[82]

Figures 17(c) and 17(d) show the plots of dc magnetic susceptibility versus temperature measured under 1000 Oe for some representative samples. In the high-temperature range, $\chi(T)$ increases with temperature decreasing down to ~ 150 K, following a Curie–Weiss law for the whole doping range $0 \leq x \leq 1$, which is similar to the scenario of $CeFeAs_{1-x}P_xO$. The values of effective moment μ_{eff} are 2.48 μ_B for $x = 0$ and 2.58 μ_B for $x = 1$ (see the inset of Fig. 17(d)), which is very close to that of a free Ce^{3+} ion, 2.54 μ_B. Actually, in the whole P doping range, μ_{eff} does not change much, and only a slightly increasing trend can be seen. At about 150 K, we observe a change in the slope of the $1/\chi$–T curve. This change can be ascribed to the CEF effect.[60] By lowering temperatures, a clear peak is observed at 2.8 K for $x = 0$, which is related to the formation of the Ce^{3+} AFM ordering. When P is doped, $\chi(T)$ increases and the peak becomes round (or shoulder-like). However, the corresponding AFM ordering temperature T_{N2} does not change much. When $x \geq 0.45$, the AFM peak disappears. Moreover, an obvious divergence between ZFC and FC is seen at low temperatures for $x > 0.6$, manifesting the simultaneous long-range FM ordered ground state of the Ce-4f electrons.

The inset in Fig. 17(c) shows the plots of magnetic susceptibility versus temperature measured under $\mu_0 H = 0.1$, 1, 3, and 5 T for the optimally doped sample ($x = 0.15$) to manifest the homogeneity of coexisting SC and Ce-4f magnetism. A small peak is observed around 3 K under 0.1 T. With external field increasing, the peak becomes rounder and more shoulder-like. Meanwhile, the peak position shifts to a lower temperature. This feature is consistent with the AFM ordering of the Ce^{3+} local moments. Furthermore, the hint of SC on $\chi(T)$ curve is suppressed by this high magnetic field.

Figure 18 shows the field dependences of magnetization at the fixed temperatures of 2 K (solid lines) and 10 K

(dashed lines), respectively. For x =0 and T =2 K, linear field-dependent magnetization is observed at low fields, while a kink is clearly seen under a moderate field, indicating a possible spin flop in the AFM state of Ce^{3+} moment.[59] When x increases, SC is enhanced. The flux pinning effect becomes more prominent and a hysteresis loop is evidently observed, as shown in Fig. 18(b). Due to the contribution from the 4f magnetism, the bean-like hysteresis loop is tilted. The AFM-correlated Ce-4f ground state persists up to $x \sim 0.45$, where $M(H)$ starts to increase rapidly for small fields and tends to be saturated at higher fields. For $0.6 \leq x \leq 0.9$, a clear FM hysteresis loop can be observed and the saturated M value reaches a maximum around $x = 0.7$ (see Fig. 18(f)). The largest saturated magnetic moment is about 0.92 μ_B/Ce, close to 1 μ_B/Ce expected for a Ce^{3+} doublet ground state.[60,70] For $x = 1$, the hysteresis loop is hardly observable down to 2 K, while the saturation tendency survives.

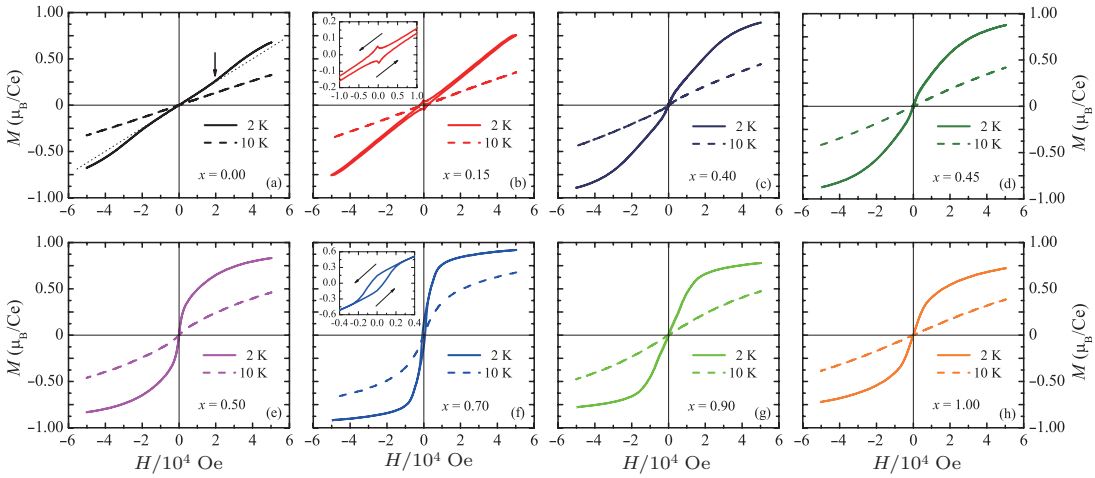


Fig. 18. Curves of isothermal magnetization $M(H)$ of $CeFeAs_{1-x}P_xO_{0.95}F_{0.05}$, measured at 2 K (solid line) and 10 K (dashed line) at (a) x =0, (b) 0.15, (c) 0.4, (d) 0.45, (e) 0.5, (f) 0.7, (g) 0.9, and (h) 1.0. The insets of panels (b) and (f) show hysteresis loops at 2 K.[82]

Therefore, both $\chi(T)$ and $M(H)$ curves exhibit a typical long-range FM ordering of the Ce^{3+} moments when $x >$ 0.6. This is consistent with previous resistivity profiles. In Fig. 16(b), a distinct inflection on $\rho(T)$ curve is clearly seen as $T < 20$ K and $x > 0.6$, indicating that the spin-flip scattering is reduced due to the formation of FM ordering. The FM correlation of Ce^{3+} moments is also supported by the negative magnetoresistance shown in the inset of Fig. 16(b).

The evolutions of electronic states can be further manifested by the specific heat measurement, as displayed in Fig. 19(a). All the five measured samples, $x = 0$, 0.15, 0.53, 0.7, and 1, show a λ-shaped peak at low temperatures, indicating a second-order phase transition. These peaks are associated with either the AFM or FM transition of the Ce-4f local moments. The residual Sommerfeld coefficient γ_0, estimated by extrapolating the C/T versus T^2 curve to the zero limit, is plotted as a function of P content x in the inset of Fig. 20. An increasing trend of γ_0 is clearly seen as P is doped, although a minimum is observed around $x = 0.15$. Since γ_0 is proportional to the DOS at the Fermi level, the small value of γ_0 at $x = 0.15$ could be due to the SC gap. The Sommerfeld coefficient for $x = 1$ is about 120.7 mJ/(mol·K^2), which is about 15 times that of $LaFePO_{0.95}F_{0.05}$ (8.3 mJ/(mol·K^2)),[83] manifesting that the correlated effect is contributed by the Ce-4f electrons. On the other hand, the presence of a magnetic peak in $C(T)$ and the absence of $-\log(T)$ behavior in the C/T versus T curve (see Fig. 21(d)), suggest that $CeFePO_{0.95}F_{0.05}$ is an enhanced correlated ferromagnet, rather than a paramagnetic HF metal.[84]

For the optimally doped $CeFeAs_{0.85}P_{0.15}O_{0.95}F_{0.05}$, the data of specific heat are further analyzed in Fig. 19(b). No obvious jump in $C(T)$ at T_{sc} can be seen from the raw data (please see the main frame), similar to the case of other 1111 systems reported previously.[85,86] The λ-shaped peak positioned at 2.9 K is attributed to the Ce^{3+} AFM transition. For the normal state, i.e., at $T > 21.5$ K, the experimental data can be well fitted by combining Debye's model and Einstein's model,[86–88] namely,

$$C(T) = \gamma T + A_D C_D(T, \theta_D) + A_E C_E(T, \theta_E), \qquad (1)$$

where γ is the Sommerfeld coefficient, $C_D(T, \theta_D)$ and $C_E(T, \theta_E)$ are Debye's function and Einstein's function, with θ_D and θ_E being their characteristic temperatures, respectively. The parameters derived from this analysis are $\gamma =$ 15.3 mJ/(mol·K^2), $\theta_D = 270.6$ K, and $\theta_E = 351.4$ K. To investigate the SC property, we subtract the fitted results from the raw data. An anomaly around T_{sc} is now clearly seen, with the jump $\Delta C/T|_{T_{sc}} \approx 5$ mJ/(mol·K^2), much smaller than those of 122 and 111 systems.[89,90] This could be attributed to the gap modulation in the k_z-axis dispersion.[91] The jump in the specific heat around T_{sc} is consistent with the large volume

fraction of magnetic shielding derived from the susceptibility. The extrapolated residual specific heat coefficient, γ_0, is 11.5 mJ/(mol·K^2). Note that this relatively large γ_0 might be contributed by magnetic impurity and/or those bands in which Cooper pair is not formed.

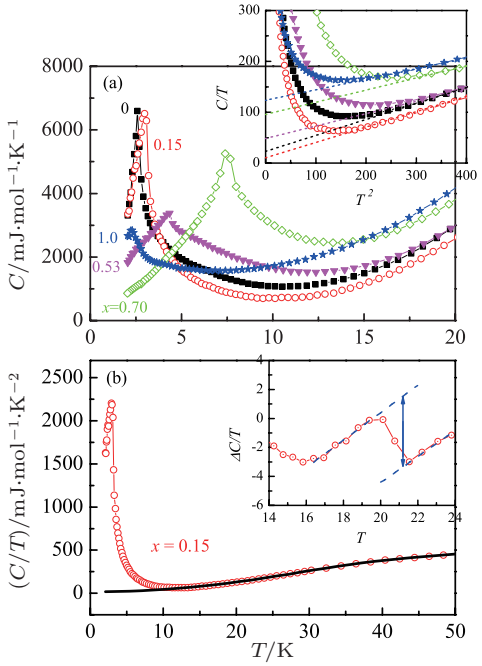


Fig. 19. (a) Plots of specific heat of $CeFeAs_{1-x}P_xO_{0.95}F_{0.05}$ versus T for $x = 0$, 0.15, 0.53, 0.7, and 1.0. The inset shows the plots of C/T versus T^2. (b) SC transition of $x = 0.15$.[82]

An electronic phase diagram is proposed to summarize the experimental results of $CeFeAs_{1-x}P_xO_{0.95}F_{0.05}$ in Fig. 20. SC is observed in the P doping range of $0 \leq x < 0.55$, with a maximal $T_{sc}^{on} \approx 21.3$ K around the optimal doping $x = 0.15$. Meanwhile, the ground state of Ce-4f local moments shows a long-range magnetic ordering, which changes from AFM to FM around $x = 0.45$. SC is found to coexist with Ce-AFM at $0 \leq x < 0.45$, and with Ce-FM at $0.45 \leq x < 0.55$, respectively. The SC re-entrances caused by the Ce-magnetism (AFM or FM) are clearly seen on the two boundaries of the SC phase, $x = 0$ and 0.53. The FM region persists to the highest P doping end $x = 1$.

We also study the physical properties of $CeFePO_{1-y}F_y$ ($y = 0$, 0.02, and 0.05), and the main experimental data are shown in Fig. 21. In general, F^- doping in CeFePO weakens the d–f correlation. a) Both susceptibility $\chi(T)$ and field-dependent magnetization $M(H)$ suggest the formation of the long-range FM ordering of Ce-4f local moment upon F doping. b) As F is doped, the crossover of coherent Kondo scattering in the $\rho(T)$ curve disappears, and it is replaced by a clear inflection at low temperatures, indicating the development of spin-flip scattering. c) A magnetic peak is observed in specific heat at $y = 0.05$, and it is far from the $-\log(T)$ behavior. These results support the previous phase diagram of $CeFeAs_{1-x}P_xO_{0.95}F_{0.05}$, where the HF behavior (which is observed in CeFePO) vanishes and the FM ordering of Ce-4f local moments emerges upon F doping in CeFePO.

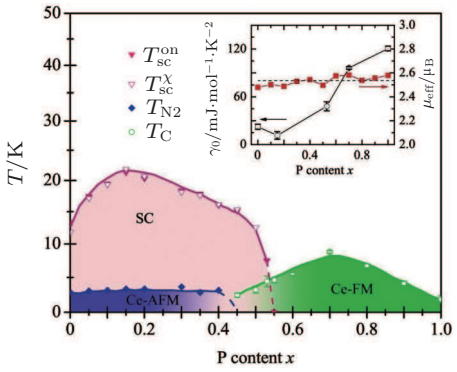


Fig. 20. Electronic phase diagram of $CeFeAs_{1-x}P_xO_{0.95}F_{0.05}$. T_{sc}^{on} and T_{sc}^{χ} come from $\rho(T)$ and $\chi(T)$, respectively. Inset shows the plots of γ_0 and μ_{eff} versus P concentration x.[82]

Now we turn to the interplay between SC and Ce-4f magnetism. While Ce-4f AFM ordering coexists with SC in a wide region $0 \leq x \leq 0.45$, in which T_{sc} reaches a maximum at about $x = 0.15$, the Ce-4f FM ordering has a strong destruction effect on SC. A slope change is clearly seen in the plot of $T_{sc}(x)$ around $x = 0.45$ as shown in Fig. 20, and T_{sc} drops significantly when Ce-4f long-range FM ordering appears. It is more interesting that once $T_C > T_{sc}$, SC vanishes almost instantly. Actually, such a re-entrant behavior in resistivity due to the 4f magnetism has also been observed in the Co-doped $EuFe_2As_2$ system,[92,93] where FM was found to coexist with SC in a narrow doping window. Furthermore, a similar first-order-like transition was also observed in $EuFe_{1.9}Co_{0.1}As_2$ under high pressure,[94] where no signature of SC could be detected once T_C is tuned to surpass T_{sc}. Since Eu^{2+} has a larger local moment, this detrimental effect of Eu^{2+} magnetism on SC is more distinct. These observations evidently point out a competition between d-electron SC pairing and Ce-4f magnetism: SC survives only when $T_{sc} > T_C$ and vanishes once the FM order is more robust.

It is also interesting to compare the two systems, $CeFeAs_{1-x}P_xO_{0.95}F_{0.05}$ and $CeFeAs_{1-x}P_xO$. While they both show the AFM-to-FM evolution of Ce-4f moments upon P doping, two main differences should be mentioned. I) SC is quite robust in 5% F-doping case, but is absent in the only P-doping case. II) The HF behavior is evident only in the P-doping case, but is not seen in the 5% F-doping case. We remark that these interesting features reflect the different roles played by the F/O and P/As substitutions, which in turn tune the 3d–4f electron correlations in a delicate way: while P/As-doping does not introduce extra electrons into the FeAs layer, but increases the intrinsic itinerancy of the d electrons and significantly enhances the inter-layer d–f coupling or Kondo effect, the effect of F/O-doping is complicated and twofold.

In the CeFeAsO end, F/O-doping introduces extra electrons into the FeAs layer, thus suppressing the d-electron AFM via band-filling effect and moderately increasing the inter-layer d–f coupling. However, in the CeFePO end, this inter-layer coupling is weakened due to F/O-doping. We find that the Kondo effect is indeed reduced in the F-doped CeFePO compounds where the HF–FM crossover is evident. Owing to the relatively large specific heat coefficient seen in Fig. 21(d), they represent a Kondo lattice system with coexistence of the partial Kondo screening and FM ordering. This feature persists in the $CeFeAs_{1-x}P_xO_{0.95}F_{0.05}$, as evidenced by the enhanced γ_0 (see the inset of Fig. 20) which reaches 50 mJ/(mol·K^2)–120 mJ/(mol·K^2), much larger than those of the La-based counterparts. This strong enhancement of Sonmerfeld coefficient should unambiguously stem from the 4f-correlation effect.

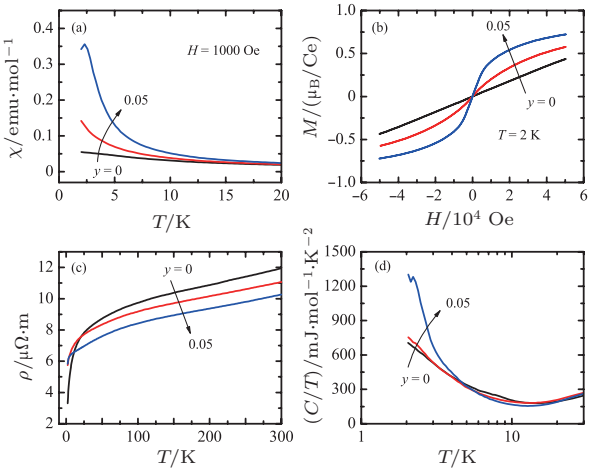


Fig. 21. Physical properties of (a) $\chi(T)$, (b) $M(H)$, (c) $\rho(T)$, and (d) C/T of $CeFePO_{1-y}F_y$, for $y = 0$ (black), 0.02 (red), and 0.05 (black).[82]

Finally, we notice a silent feature of the F-doping case: although the ionic radius of F^- (1.33 Å) is smaller than that of O^{2-} (1.40 Å),[95] the c axis of $CeFeAs_{1-x}P_xO_{0.95}F_{0.05}$ is larger than that of $CeFeAs_{1-x}P_xO$ as $x > 0.45$ (see the inset of Fig. 15). This supports the previous expectation that the Kondo coupling becomes weaker in CeFePO when F^- is doped. As is well known, compared with FeAs-based compounds, FeP-based compounds exhibit very obvious tridimensionality.[41] A two-dimensional (2D) hole cylinder present in the former case transforms into a pocket with three-dimensional (3D) dispersion in the latter. As F^- is doped, extra electrons are introduced, and it is possible that the small 3D pocket firstly diminishes, leaving only 2D FS's and leading to a weakened inter-layer d–f coupling. This is one possible interpretation to the slight increase of c axis in the CeFePO end, and it should be responsible for the absence of HF behavior in the $CeFePO_{0.95}F_{0.05}$.

6. $CeFeAsO_{1-y}F_y$ under pressure

For comparison, we here present the result of physical pressure effect of CeFeAsO which was shown by Zocco *et al.*[96] The authors applied both hydrostatic and anvil pressures. Figure 22(a) shows the plots of resistivity versus temperature of CeFeAsO with diamond anvil pressure cell. One may find that the hump associated with structural distortion and/or Fe-AFM is suppressed by external pressure, and at very high pressure, the system evolves into a typical Kondo lattice behavior. For example, $\rho(T)$ decreases slowly at high temperature, and drops much faster below the Kondo-coherence temperature, T_0. It is well known that in Ce-contained compounds, pressure increases the value of the hybridization matrix element V_{fc} between 4f and conduction electrons,[97] leading to an increase in T_0. Fermi-liquid-like temperature–resistivity correlation was observed well below T_0. All these observations are within the expectation of a pressure effect, and are generally compatible with the chemical pressure effect. The authors did not observe any evidence of SC for all the measured pressures and temperatures.

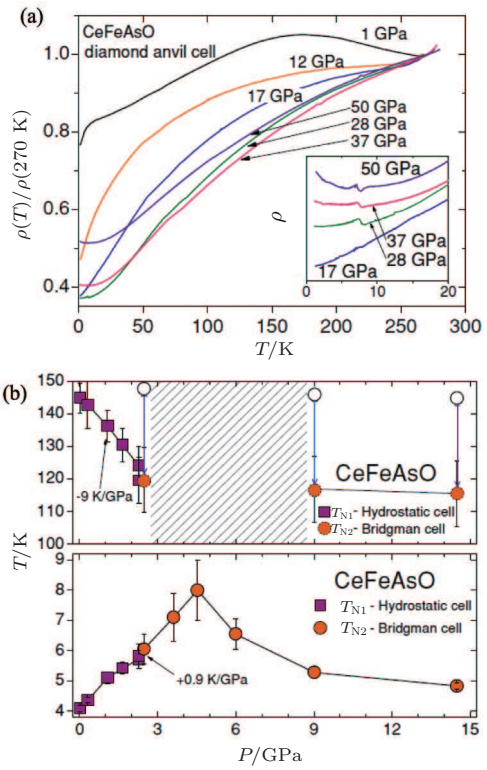


Fig. 22. (a) Temperature dependences of resistivity of CeFeAsO under various pressures. (b) Phase diagram of CeFeAsO under pressure.[96]

However, we should also mention the differences between physical pressure effect and chemical pressure effect on CeFeAsO. First, the AFM transition associated with 3d electrons on $\rho(T)$ curve is hardly resolvable when p exceeds 3 GPa, and this leaves us a question of whether this Fe-AFM ordering will be continuously suppressed by external pressure and results in a QCP. Second, the ordering temperature of Ce-AFM

under pressure goes up substantially before dropping down, although the authors were not able to detect a transformation from AFM to FM directly. In the chemical pressure case, T_{N2} does not change too much with P doping concentration. One possibility is that the chemical pressure is more isotropic than the external pressure, so that the enhancement of J_{RKKY} by shortening the c axis is somewhat partially cancelled by the enhancement of $J_f^{(0)}$ caused by squeezing within ab plane. Third, at high external pressures, it seems that the system has entered a mixed-valence regime, and thus goes much farther than the P/As-doping chemical pressure effect. Besides, there is a minimum and a tiny upturn in $\rho(T)$ at low temperatures under very high pressure, of which the mechanisms are still unclear.

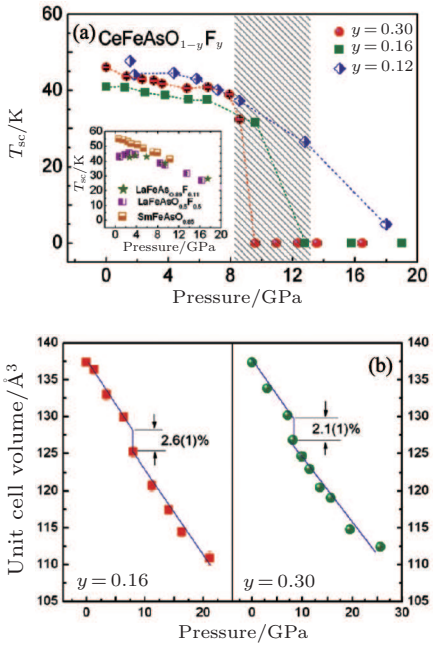


Fig. 23. (a) Pressure dependence of T_{sc} of CeFeAsO$_{1-y}$F$_y$ ($y = 0.16$ and 0.3) samples. (b) Pressure dependence of the unit cell volume for $y = 0.16$ and $y = 0.3$ samples.[98]

For superconducting samples of CeFeAsO$_{1-y}$F$_y$ under pressure, people have focused on the optimally doped and over-doped samples.[98,99] For both of them, external pressure suppresses T_{sc} (see Fig. 23(a)), which is in contrast to the chemical pressure effect in the F^- under-doped case on which we have reported in Section 5. One attractive feature of CeFeAsO$_{1-y}$F$_y$ under pressure is that near the first-order phase transition of SC to non-SC, the authors also discovered a sudden volume collapse, as shown in Fig. 23(b). Further X-ray absorption spectroscopy (XAS) measurement confirms a valence change of Ce ions, suggesting a pressure-induced competition between SC and Kondo effect. If we summarize all the physical/chemical pressure effects on different F^- doping regions of CeFeAsO$_{1-y}$F$_y$, we will obtain a doping dependence of pressure effect, i.e., pressure fails to induce SC in parent compound, but enhances SC in the under-doped CeFeAsO$_{1-y}$F$_y$, while reduces SC for both optimal- and over-doped cases. Here we should mention that the pressure may be used to affect the electronic properties of CeFeAsO in a significantly different manner from chemical substitution, and is also distinct from the pressure effect in LaFeAsO,[38] providing more evidences for the interplay between SC and d–f correlation. Whereas the pressure effect on under-doped CeFeAsO$_{1-y}$F$_y$ is still lacking, it might be too early to draw an accurate conclusion before further investigation has been performed in the future.

7. Conclusions and perspectives

To provide a comprehensive understanding of the interplay between rare-earth magnetism and SC in iron-based superconductor, we review recent advances in the study of the P/As-doping chemical pressure effect on CeFeAsO$_{1-y}$F$_y$. The conclusions are listed as follows.

(I) The P/As-doping in CeFeAsO$_{1-y}$F$_y$ acts as an effective controlling parameter to tune the electronic and magnetic properties. With this chemical pressure, we derive two magnetic critical points in CeFeAs$_{1-x}$P$_x$O, i.e., $x_{c1} \simeq 0.4$ for suppression of Fe-AFM ordering, and $x_{c2} \simeq 0.92$ for disappearance of Ce-FM ordering. Besides, the magnetic ground state of Ce^{3+} moments changes from AFM ordering in CeFeAsO to FM ordering which gives rise to a transition point $x_{c3} \simeq 0.37$. Heavy fermion behavior is confirmed for $x > x_{c2}$. We illustrate this phase diagram by extending Doniach's picture,[80] in which the original competitor (i.e., J_{RKKY}) of Kondo effect is replaced by the total exchange $J_f = J_f^{(0)} + J_{RKKY}$. In the CeFeAs$_{1-x}P_xO_{0.95}F_{0.05}$ case, x_{c1} moves towards left-hand side and is estimated to be ~ 0.15, while x_{c3} slightly changes from 0.37 to 0.45. The 5% F doping also drives x_{c2} out of the phase diagram, leaving CeFePO$_{0.95}$F$_{0.05}$ with an enhanced correlated ferromagnet.

(II) Comparison of the phase diagrams between CeFeAs$_{1-x}$P$_x$O and CeFeAs$_{1-x}$P$_x$O$_{0.95}$F$_{0.05}$ indicates that the most striking difference is that a broad SC region exists in the latter, while absent in the former. Since CeFeAsO$_{0.95}$F$_{0.05}$ is on the boundary to SC, such a robust SC region in CeFeAs$_{1-x}$P$_x$O$_{0.95}$F$_{0.05}$ manifests that chemical pressure enhances SC in CeFeAs$_{1-x}$P$_x$O$_{0.95}$F$_{0.05}$. The absence of SC in CeFeAs$_{1-x}$P$_x$O where $x_{c1} \simeq x_{c3}$ and the appearance of SC in CeFeAs$_{1-x}$P$_x$O$_{0.95}$F$_{0.05}$ where x_{c1} and x_{c3} are separate strongly demonstrate the interplay between Ce-magnetism and SC. This can be concluded as: Ce-AFM ordering coexists with SC harmoniously while Ce-FM ordering competes with SC, and SC appears only if $T_{sc} > T_C$.

(III) Another important feature of CeFeAs$_{1-x}$P$_x$O$_{0.95}$F$_{0.05}$ is the disappearance of HF behavior on the phase diagram. We describe this with the right-hand movement of x_{c2}. This phenomenon is consistent with the tiny lattice expansion in the

CeFePO end by F^- doping (see the inset of Fig. 15), even though the ionic radius of F^- is smaller than that of O^{2-}. We ascribe this to the selective band-filling effect of F^- doping that diminishes the small 3D hole FS pocket with only 2D FS sheets left, and therefore weakens the inter-layer hybridization.

There are many aspects of problems that still need to be clarified in the future. The first problem is about the possible SC emergence in $CeFeAs_{1-x}P_xO$. In our poly-crystalline samples, SC is not observed on the whole phase diagram down to 2 K, but this is still a challenge to lower temperatures in single crystals. Jesche *et al.*[100] recently reported the observation of SC at around 3.7 K in single crystalline $CeFeAs_{0.7}P_{0.3}O$. It is doubtful that the T_{sc} is so coincident with that of Sn which was used as the flux. Better single crystals are still highly necessary to settle this divergence. The second problem is about the nature of Ce-FM QCP. Note that a genuine FM QCP is extremely rare.[101] In most cases, FM moments form AFM ordering[102] or Kondo-cluster-glass[103] before reaching a real FM QCP. The recent experiment[104] has claimed that short-range static magnetism in CeFePO occurs below the freezing temperature $T_g \simeq 0.7$ K, which prevents the system from accessing the putative FM QCP. Hence, it will be of great interest to carry out more studies to elucidate the nature of Ce-FM QCP in $CeFeAs_{1-x}P_xO$. The third problem as mentioned above is that an AFM ordering induced SC re-entrance is rare. Usually, an FM ordering with $T_C < T_{sc}$ is likely to cause an SC re-entrance, as are the cases in $EuFe_2(As_{0.7}P_{0.3})_2$[105] and $LnNi_2B_2C$ (Ln = Tm, Er, Ho).[106] However, an AFM case is rare and the mechanism is still now unclear. The possible interpretation of FM component from canted Ce^{3+} moments still needs to be identified by more advanced techniques such as neutron scattering experiment.

References

[1] Kamihara Y, Watanabe T, Hirano M and Hosono H 2008 *J. Am. Chem. Soc.* **130** 3296

[2] Kamihara Y, Hiramatsu H, Hirano M, Kawamura R, Yanagi H, Kamiya T and Hosono H 2006 *J. Am. Chem. Soc.* **128** 10012

[3] Chen X H, Wu T, Wu G, Liu R H, Chen H and Fang D F 2008 *Nature* **453** 761

[4] Chen G F, Li Z, Wu D, Li G, Hu W Z, Dong J, Zheng P, Luo J L and Wang N L 2008 *Phys. Rev. Lett.* **100** 247002

[5] Wen H H, Mu G, Fang L, Yang H and Zhu X 2008 *Europhys. Lett.* **82** 17009

[6] Ren Z A, Yang J, Lu W, Yi W, Che G C, Dong X L, Sun L L and Zhao Z X 2008 *Mater. Res. Innov.* **12** 105

[7] Ren Z A, Lu W, Yang J, Yi W, Shen X L, Zheng C, Che G C, Dong X L, Sun L L, Zhou F and Zhao Z X 2008 *Chin. Phys. Lett.* **25** 2215

[8] Takahashi H, Igawa K, Arii K, Kamihara Y, Hirano M and Hosono H 2008 *Nature* **453** 376

[9] Ren Z, Che G, Dong X, Yang J, Lu W, Yi W, Shen X, Li Z, Sun L, Zhou F and Zhao Z 2008 *Europhys. Lett.* **83** 17002

[10] Wang C, Li L, Chi S, Zhu Z, Ren Z, Li Y, Wang Y, Lin X, Luo Y, Xu X, Cao G and Xu Z 2008 *Europhys. Lett.* **83** 67006

[11] Li L J, Li Y K, Ren Z, Luo Y K, Lin X, He M, Tao Q, Zhu Z W, Cao G H and Xu Z A 2008 *Phys. Rev. B* **78** 132506

[12] Yang J, Shen X L, Lu W, Yi W, Li Z C, Ren Z A, Che G C, Dong X L, Sun L L, Zhou F and Zhao Z X 2009 *New J. Phys.* **11** 025005

[13] Rotter M, Tegel M and Johrendt D 2008 *Phys. Rev. Lett.* **101** 107006

[14] Hsu F C, Luo J Y, Yeh K W, Chen T K, Huang T W, Wu P W, Lee Y C, Huang Y L, Chu Y Y, Yan D C and Wu M K 2008 *Proc. Natl. Acad. Sci. USA* **105** 14262

[15] Fang M H, Pham H M, Qian B, Liu T H, Vehstedt E K, Liu Y, Spinu L and Mao Z Q 2008 *Phys. Rev. B* **78** 224503

[16] Wang X C, Liu Q Q, Lü Y X, Gao W B, Yang L X, Yu R C, Li F Y and Jin C Q 2008 *Solid State Commun.* **148** 538

[17] Tegel M, Johansson S, Weiss V, Schellenberg I, Hermes M, Pöttgen R and Johrendt D 2008 *Europhys. Lett.* **84** 67007

[18] Guo J, Jin S, Wang G, Wang S, Zhu K, Zhou T, He M and Chen X 2010 *Phys. Rev. B* **82** 180520(R)

[19] Pitcher M J, Parker D R, Adamson P, Herkelrath S J C, Boothroyd A T and Clarke S J 2008 *Chem. Commun.* **45** 5918

[20] Pottgen R and Johrent D 2008 *Z. Natureforsch.* **63b** 1135

[21] Zhu X, Han F, Mu G, Cheng P, Shen B, Zeng B and Wen H H 2009 *Phys. Rev. B* **79** 220512

[22] Zhu X, Han F, Mu G, Zeng B, Cheng P, Shen B and Wen H H 2009 *Phys. Rev. B* **79** 024516

[23] Tomita Y, Kotegawa H, Tao Y, Tou H, Ogino H, Horii S, Kishio K and Shimoyama J 2012 *Phys. Rev. B* **86** 134527

[24] Ogino H, Sato S, Kishio K, Shimoyama J, Tohei T and Ikuhara Y 2010 *Appl. Phys. Lett.* **97** 072506

[25] Klimczuk T, McQueen T M, Williams A J, Huang Q, Ronning F, Bauer E D, Thompson J D, Green M A and Cava R J 2009 *Phys. Rev. B* **79** 012505

[26] Sun L, Chen X J, Guo J, Gao P, Huang Q Z, Wang H, Fang M, Chen X, Chen G, Wu Q, Zhang C, Gu D, Dong X, Wang L, Yang K, Li A, Dai X, Mao H, and Zhao Z 2012 *Nature* **483** 67

[27] de la Cruz C, Huang Q, Lynn J W, Li J, Ratcliff II W, Zarestky J L, Mook H A, Chen G F, Luo J L, Wang N L and Dai P 2008 *Nature* **453** 899

[28] Klauss H H, Luetkens H, Klingeler R, Hess C, Litterst F J, Kraken M, Korshunov M M, Eremin I, Drechsler S L, Khasanov R, Amato A, Borrero J H, Leps N, Kondrat A, Behr G, Werner J and Büchner B 2008 *Phys. Rev. Lett.* **101** 077005

[29] Kitao S, Kobayashi Y, Higashitaniguchi S, Saito M, Kamihara Y, Hirano M, Mitsui T, Hosono H and Seto M 2008 *J. Phys. Soc. Jpn.* **77** 103706

[30] Nakai Y, Ishida K, Kamihara Y, Hirano M and Hosono H 2008 *J. Phys. Soc. Jpn.* **77** 073701

[31] Yildirim T 2008 *Phys. Rev. Lett.* **101** 057010

[32] Si Q M and Abrahams E 2008 *Phys. Rev. Lett.* **101** 076401

[33] Fang C, Yao H, Tsai W F, Hu J P and Kivelson S A 2008 *Phys. Rev. B* **77** 224509

[34] Seo K, Bernevig B A and Hu J P 2008 *Phys. Rev. Lett.* **101** 206404

[35] Bednorz J G and Müller K A 1986 *Z. Phys.* **B64** 189

[36] Lee P A 2006 *Rev. Mod. Phys.* **78** 17

[37] Luetkens H, Klauss H H, Kraken M, Litterst F J, Dellmann T, Klingeler R, Hess C, Khasanov R, Amato A, Baines C, Kosmala M, Schumann O J, Braden M, Hamann-Borrero J, Leps N, Kondrat A, Behr G, Werner J and Büchner B 2009 *Nat. Mater.* **8** 305

[38] Okada H, Igawa K, Takahashi H, Kamihara Y, Hirano M, Hosono H, Matsubayashi K and Uwatoko Y 2008 *J. Phys. Soc. Jpn.* **77** 113712

[39] Mani A, Ghosh N, Paulraj S, Bharathi A and Sundar C S 2009 *Europhys. Lett.* **87** 17004

[40] Pearson W B 1972 *Crystal Chemistry and Physics of Metals and Alloys* (New York: Wiley Interscience)

[41] Vildosola V, Pourovskii L, Arita R, Biermann S and Georges A 2008 *Phys. Rev. B* **78** 064518

[42] Hertz J A 1976 *Phys. Rev. B* **14** 1165

[43] Dai J, Si Q, Zhu J X and Abrahams E 2009 *Proc. Natl. Acad. Sci. USA* **106** 4118

[44] Pourovskii L, Vildosola V, Biermann S and Georges A 2008 *Europhys. Lett.* **84** 37006

[45] Wang C, Jiang S, Tao Q, Ren Z, Li Y, Li L, Feng C, Dai J, Cao G and Xu Z 2009 *Europhys. Lett.* **86** 47002

[46] Jiang S, Xing H, Xuan G, Wang C, Ren Z, Feng C, Dai J, Xu Z and Cao G 2009 *J. Phys.: Condens. Matter* **21** 382203

[47] Kasahara S, Shibauchi T, Hashimoto K, Ikada K, Tonegawa S, Okazaki R, Shishido H, Ikeda H, Takeya H, Hirata K, Terashima T and Matsuda Y 2010 *Phys. Rev. B* **81** 184519

[48] Shishido H, Bangura A F, Coldea A I, Tonegawa S, Hashimoto K, Kasahara S, Rourke P M C, Ikeda H, Terashima T, Settai R, Ōnuki Y, Vignolles D, Proust C, Vignolle B, McCollam A, Matsuda Y, Shibauchi T and Carrington A 2010 *Phys. Rev. Lett.* **104** 057008

[49] Hewson A C 1993 *The Kondo Problem to Heavy Fermions* (Cambridge: Cambridge University Press)

[50] Luo Y, Han H, Tan H, Lin X, Li Y, Jiang S, Feng C, Dai J, Cao G, Xu Z and Li S 2011 *J. Phys.: Condens. Matter* **23** 175701

[51] Luo Y, Pourovskii L, Rowley S, Li Y, Feng C, Georges A, Dai J, Cao G, Xu Z, Si Q and Ong N P (to be published)

[52] Krellner C, Burkhardt U and Geibel C 2009 *Physica B* **404** 3206

[53] Ohta H and Yoshimura K 2009 *Phys. Rev. B* **80** 184409

[54] Sarkar B, Jesche A, Krellner C, Baenitz M and Geibel C 2010 *Phys. Rev. B* **82** 054423

[55] Krellner C, Kini N S, Brüuning E M, Koch K, Rosner H, Nicklas M, Baenitz M and Geibel C 2007 *Phys. Rev. B* **76** 104418

[56] Singh D J and Du M H 2008 *Phys. Rev. Lett.* **100** 237003

[57] Zhao J, Huang Q, de la Cruz C, Li S, Lynn J W, Chen Y, Green M A, Chen G F, Li G, Li Z, Luo J L, Wang N L and Dai P 2008 *Nat. Mater.* **7** 953

[58] Sefat A S, Huq A, McGuire M A, Jin R, Sales B C, Mandrus D, Cranswick L M D, Stephens P W and Stone K H 2008 *Phys. Rev. B* **78** 104505

[59] Jesche A, Krellner C, de Souza M, Lang F and Geibel C 2009 *New J. Phys.* **11** 103050

[60] Brüning E M, Krellner C, Baenitz M, Jesche A, Steglich F and Geibel C 2008 *Phys. Rev. Lett.* **101** 117206

[61] McQueen T M, Regulacio M, Williams A J, Huang Q, Lynn J W, Hor Y S, West D, Green M A and Cava R J 2008 *Phys. Rev. B* **78** 024521

[62] Kitagawa S, Ikeda H, Nakai Y, Hattori T, Ishida K, Kamihara Y, Hirano M and Hosono H 2011 *Phys. Rev. Lett.* **107** 277002

[63] Schröder A, Aeppli G, Coldea R, Adams M, Stockert O, Löhneysen H V, Bucher E, Ramazashill R and Coleman P 2000 *Nature* **407** 351

[64] Si Q M, Ingersent K and Smith J L 2001 *Nature* **413** 804

[65] Coleman P 2007 "Heavy Fermion: Electrons at the Edge of Magnetism", in *Handbook of Magnetism and Advanced Magnetic Materials*, ed. Kronmuller H and Parkin S, Vol. 1, (New York: Wiley) pp. 95–148

[66] Luo Y, Li Y, Jiang S, Dai J, Cao G and Xu Z 2010 *Phys. Rev. B* **81** 134422

[67] Lu D H, Yi M, Mo S K, Erickson A S, Analytis J, Chu J H, Singh D J, Hussain Z, Geballe T H, Fisher I R and Shen Z X 2008 *Nature* **455** 81

[68] Hess C, Kondrat A, Narduzzo A, Hamann-Borrero J E, Klingeler R, Werner J, Behr G and Büchner B 2009 *Europhys. Lett.* **87** 17005

[69] de la Cruz C, Hu W Z, Li S, Huang Q, Lynn J W, Green M A, Chen G F, Wang N L, Mook H A, Si Q and Dai P 2010 *Phys. Rev. Lett.* **104** 017204

[70] Chi S, Adroja D T, Guidi T, Bewley R, Li S, Zhao J, Lynn J W, Brown C M, Qiu Y, Chen G F, Lou J L, Wang N L and Dai P 2008 *Phys. Rev. Lett.* **101** 217002

[71] Huntelaar M E, Booij A S, Cordfunke E H P and van der Laan R R 2000 *J. Chem. Thermodyn.* **32** 465

[72] Dai J, Zhu J X and Si Q 2009 *Phys. Rev. B* **80** 020505

[73] Qazilbash M M, Hamlin J J, Baumbach R E, Zhang L, Singh D J, Maple M B and Basov D N 2009 *Nat. Phys.* **5** 647

[74] Maeter H, Luetkens H, Pashkevich Y G, Kwadrin A, Khasanov R, Amato A, Gusev A A, Lamonova K V, Chervinskii D A, Klingeler R, Hess C, Behr G, Büchner B and Klauss H H 2009 *Phys. Rev. B* **80** 094524

[75] Ruderman M and Kittel C 1954 *Phys. Rev.* **96** 99

[76] Kasuya T 1956 *Prog. Theor. Phys.* **16** 45

[77] Yosida K 1956 *Phys. Rev.* **106** 893

[78] Si Q and Abrahams E 2008 *Phys. Rev. Lett.* **101** 076401

[79] Si Q, Abrahams E, Dai J and Zhu J X 2009 *New J. Phys.* **11** 045001

[80] Doniach S 1977 *Physica B* **91** 231

[81] Nevidomskyy A H and Coleman P 2009 *Phys. Rev. Lett.* **103** 147205

[82] Luo Y, Han H, Jiang S, Lin X, Li Y, Dai J, Cao G and Xu Z 2011 *Phys. Rev. B* **83** 054501

[83] Suzuki S, Miyasaka S, Tajima S, Kida T and Hagiwara M 2009 *J. Phys. Soc. Jpn.* **78** 114712

[84] Stewart G R 1984 *Rev. Mod. Phys.* **56** 755

[85] Mu G, Zhu X Y, Fang L, Shan L, Ren C and Wen H H 2008 *Chin. Phys. Lett.* **25** 2221

[86] Baker P J, Giblin S R, Pratt F L, Liu R H, Wu G, Chen X H, Pitcher M J, Parker D R, Clarke S J and Blundell S J 2009 *New J. Phys.* **11** 025010

[87] Tropeano M, Martinelli A, Palenzona A, Bellingeri E, Galleani d'Agliano E, Nguyen T D, Affronte M and Putti M 2008 *Phys. Rev. B* **78** 094518

[88] Drew A J, Niedermayer C, Baker P J, Pratt F L, Blundell S J, Lancaster T, Liu R H, Wu G, Chen X H, Watanabe I, Malik V K, Dubroka A, Rössle M, Kim K W, Baines C and Bernhard C 2009 *Nat. Mater.* **8** 310

[89] Mu G, Luo H, Wang Z, Shan L, Ren C and Wen H H 2009 *Phys. Rev. B* **79** 174501

[90] Wei F, Chen F, Sasmal K, Lü B, Tang Z J, Xue Y Y, Guloy A M and Chu C W 2010 *Phys. Rev. B* **81** 134527

[91] Reid J P, Tanatar M A, Luo X G, Shakeripour H, Leyraud N D, Ni N, Bud'ko S L, Canfield P C, Prozorov R and Taillefer L 2010 *Phys. Rev. B* **82** 064501

[92] Jiang S, Xing H, Xuan G, Ren Z, Wang C, Xu Z and Cao G 2009 *Phys. Rev. B* **80** 184514

[93] He Y, Wu T, Wu G, Zheng Q J, Liu Y Z, Chen H, Ying J J, Liu R H, Wang X F, Xie Y L, Yan Y L, Dong J K, Li S Y and Chen X H 2010 *J. Phys.: Condens. Matter* **22** 235701

[94] Nicklas M, Kumar M, Lengyel E, Schnelle W and Leithe-Jasper A 2011 *J. Phys.: Conf. Ser.* **273** 012101

[95] Shannon R D 1976 *Acta Crystallogr. A* **32** 751

[96] Zocco D A, Baumbach R E, Hamlin J J, Janoschek M, Lum I K, McGuire M A, Sefat A S, Sales B C, Jin R, Mandrus D, Jeffries J R, Weir S T, Vohra Y K and Maple M B 2011 *Phys. Rev. B* **83** 094528

[97] Maple M B, Wohlleben D K, Jr C D G and R J J 1973 *Magnetism and Magnetic Materials* (New York: AIP)

[98] Zocco D A, Hamlin J J, Baumbach R E, Maple M B, McGuire M A, Sefat A S, Sales B C, Jin R, Mandrus D, Jeffries J R, Weir S T and Vohra Y K 2008 *Physica C* **468** 2229

[99] Sun L, Dai X, Zhang C, Yi W, Chen G, Wang N, Zheng L, Jiang Z, Wei X, Huang Y, Yang J, Ren Z, Lu W, Dong X, Che G, Wu Q, Ding H, Liu J, Hu T and Zhao Z 2010 *Europhys. Lett.* **91** 57008

[100] Jesche A, Förster T, Spehling J, Nicklas M, Souza M de, Gumeniuk R, Luetkens H, Goltz T, Krellner C, Lang M, Sichelschmidt J, Klauss H H and Geibel C 2012 *Phys. Rev. B* **86** 020501

[101] Stewart G R 2001 *Rev. Mod. Phys.* **73** 797

[102] Süllow S, Aronson M C, Rainford B D and Haen P 1999 *Phys. Rev. Lett.* **82** 2963

[103] Westerkamp T, Deppe M, Küchler R, Brando M, Geibel C, Gegenwart P, Pikul A P and Steglich F 2009 *Phys. Rev. Lett.* **102** 206404

[104] Lausberg S, Spehling J, Steppke A, Jesche A, Luetkens H, Amato A, Baines C, Krellner C, Brando M, Geibel C, Klauss H H and Steglich F 2012 *Phys. Rev. Lett.* **109** 216402

[105] Ren Z, Tao Q, Jiang S, Feng C, Wang C, Dai J, Cao G and Xu Z 2009 *Phys. Rev. Lett.* **102** 137002

[106] Eisaki H, Takagi H, Cava R J, Batlogg B, Krajewski J J, Peck W F Jr, Mizuhashi K, Lee J O and Uchida S 1994 *Phys. Rev. B* **50** 647